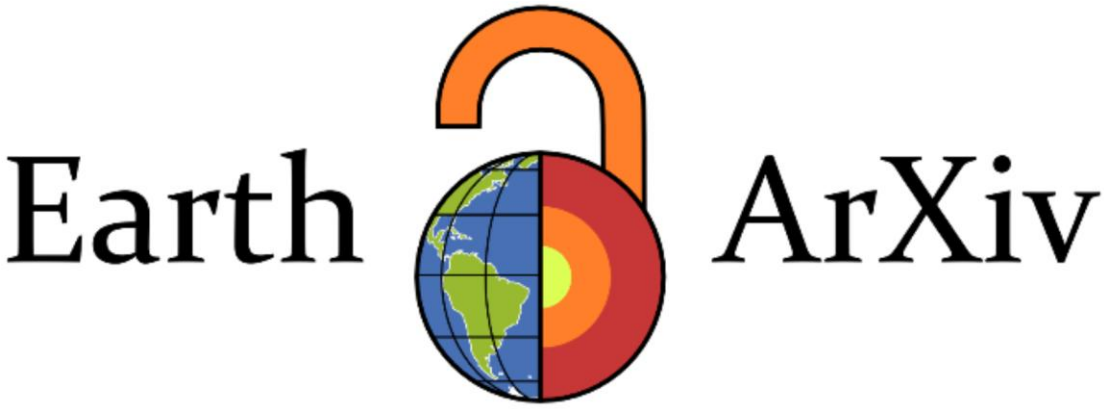

Development of a dynamic true triaxial electromagnetic Hopkinson bar system

Heping Xie[1,2], Jianbo Zhu[1,2]*, Yulong Li[3], Tao Zhou[1,2], Weiyue Bao[1,2], Shiwei Zhang[1,2], Zhongbin Tang[3], Tao Suo[3], Xiaoyong Song[1,2], Jian Zhao[4]

[1] State Key Laboratory of Intelligent Construction and Healthy Operation and Maintenance of Deep Underground Engineering, College of Civil and Transportation Engineering, Shenzhen University, Shenzhen, 518060, China

[2] Guangdong Provincial Key Laboratory of Deep Earth Sciences and Geothermal Energy Exploitation and Utilization, Institute of Deep Earth Sciences and Green Energy, College of Civil and Transportation Engineering, Shenzhen University, Shenzhen, 518060, China

[3] School of Aeronautics, Northwestern Polytechnical University, 127 Youyi West Road, Xi'an 710072, China

[4] Department of Civil Engineering, Monash University, Melbourne, VIC 3800, Australia

* Corresponding authors; Emails: jianbo.zhu@szu.edu.cn

Peer review status:

This is a non-peer-reviewed preprint submitted to EarthArXiv.

This manuscript is to be submitted to the International Journal of Rock Mechanics and Mining Sciences.

Development of a dynamic true triaxial electromagnetic Hopkinson bar system

Heping Xie[1,2], Jianbo Zhu[1,2]*, Yulong Li[3], Tao Zhou[1,2], Weiyue Bao[1,2], Shiwei Zhang[1,2], Zhongbin Tang[3], Tao Suo[3], Xiaoyong Song[1,2], Jian Zhao[4]

[1] State Key Laboratory of Intelligent Construction and Healthy Operation and Maintenance of Deep Underground Engineering, College of Civil and Transportation Engineering, Shenzhen University, Shenzhen, 518060, China

[2] Guangdong Provincial Key Laboratory of Deep Earth Sciences and Geothermal Energy Exploitation and Utilization, Institute of Deep Earth Sciences and Green Energy, College of Civil and Transportation Engineering, Shenzhen University, Shenzhen, 518060, China

[3] School of Aeronautics, Northwestern Polytechnical University, 127 Youyi West Road, Xi'an 710072, China

[4] Department of Civil Engineering, Monash University, Melbourne, VIC 3800, Australia

* Corresponding authors; Emails: jianbo.zhu@szu.edu.cn

Abstract: Subsurface rock masses and rock engineering are typically subjected to multiaxial static stresses, often superimposed by multidirectional dynamic disturbances induced by seismic events, blast loading and mechanical vibrations, etc. A comprehensive understanding of the dynamic mechanical behavior and failure mechanisms of rocks under such coupled multiaxial or three-dimensional static and dynamic loading conditions is critical for the rational design, safe construction and long-term stability of rock engineering projects. However, there has been no three-dimensional dynamic theory of rock so far. A major reason is the lack of dynamic true triaxial apparatus. To address this need, we developed a novel cutting-edge testing platform, i.e., dynamic true triaxial electromagnetic Hopkinson bar (DTEHB) system. It is the first apparatus in the world for studying dynamic responses of rock masses under coupled three-dimensional dynamic disturbances and true triaxial static in situ stresses. The fundamental working principles, system configuration and key technical challenges overcome in the development of the DTEHB are introduced in detail in this paper. By combining electromagnetic energy conversion and synchronous control techniques, the DTEHB achieves highly repeatable (>99%) and precise true triaxial synchronous impact loading, and synchronous six-directional dynamic loading (time error ≤5 μs). The DTEHB system is also capable of simulating coupled triaxial/six-directional impact and static confining pressure loading, replicating 3D in situ stress conditions. Moreover, the system's reliability and performance are validated through analyzing controlled and adjustable stress waveforms (repeatability, duration, amplitude and arrival time), static true triaxial confining pressures and synchronous generation and arrival six-directional

stress pulses. Dynamic true triaxial synchronized impact tests were successfully conducted on rock specimens for the first time. The establishment of the DTEHB could facilitate experimental testing of rock and other materials under a range of dynamic disturbances, thereby advancing the theory of three-dimensional rock dynamic theories.

Keywords： Rock dynamics; DTEHB; Dynamic true triaxial loading; Synchronous control

1. Introduction

With increasing global demands for energy, resource exploitation, and transportation infrastructure, a growing number of rock engineering projects are being constructed-or planned-in deep underground environments characterized by high and complex crustal stresses, as well as active dynamic disturbances. In such settings, subsurface rock masses and engineered structures are subjected to true triaxial static stresses, often coupled with multi-directional dynamic loads induced by seismic activity, blasting, and mechanical vibrations. Under these conditions, the dynamic disasters, such as rockbursts, coal bumps, and large-scale collapses, frequently occur with the characteristics of sudden and extremely destructive, which induced significant risks during construction and operation (Ranjith et al. 2017; Rehbock-Sander and Jesel 2018; Xie et al. 2019, 2020). In general, these hazards associated with such dynamic disasters are difficult to predict and prevent. Hence, an adequate understanding of rock dynamic behavior-particularly under multi-axial static and dynamic loading conditions-is vital for guaranteeing the safety and stability of deep underground engineering structures.

Laboratory testing is a fundamental and widely adopted methodology for studying the dynamic mechanical and failure behavior of rocks under complex dynamic loading. There are various experimental techniques that have been developed to describe rock dynamic responses at different strain rates, including hydraulic/stress servo-controlled systems (Fairhurst and Hudson 1999; Olsson 1991), drop weight device (Reddish et al. 2005; Whittles et al. 2006), split Hopkinson pressure bar (SHPB) (Kolsky 1963; Zhao and Gary 1996) and planar impact machine (Ahrens and Rubin 1993). Among these, SHPB has emerged as the most prevalent method for dynamic rock testing at intermediate to high strain rates (10^1~10^3 s^{-1}), owing to its well-established theoretical framework and experimental reliability.

The SHPB was first introduced by Kumar (1968) for characterizing dynamic behavior of rocks and has since been widely employed in rock dynamics research (Doan and Gary 2009; Frew et al. 2001; Goldsmith et al. 1976; Ju et al. 2007; Lambert and Ross 2000; Li et al. 2005, 2017a, 2017b; Lindholm et al. 1974; Lu et al. 2010; Melosh et al. 1992; Olsson 1991; Perkins et al. 1970; Qi et al. 2019; Wang et al. 2009, 2017, 2018; Wu et al. 2016; Xia and Yao 2015; Xie and Sanderson 1996; Yuan et al. 2011; Zhang and Zhao 2013, 2014; Zhou et al. 2018, 2020; Zhu et al. 2018a). These studies

have established that the mechanical response and failure mechanisms of rocks are strain-rate dependent. However, as aforementioned, rock masses in engineering practices are usually subjected to combined complex static in situ stresses and dynamic disturbances, a loading condition that conventional SHPB system cannot replicate. To overcome this limitation, several modifications to the SHPB have been proposed in recent years. In a pioneering study, Li et al. (2008) developed an axisymmetric triaxial confined SHPB, enabling dynamic loading along one axis while maintaining static confining pressures ($\sigma_1 \geqslant \sigma_2 = \sigma_3 \neq 0$, where σ_1, σ_2 and σ_3 are principal stresses). An alternative approach is to use a transverse constraint ring to achieve axial symmetry confinement during axial dynamic loading (Chen and Ravichandran 1997; Chen and Song 2011). For more complex stress states, Zhao and Cadoni (2009) conceptualized a modified SHB capable of imposing a static true triaxial stress ($\sigma_1 \geqslant \sigma_2 \geq \sigma_3 \neq 0$) before dynamic impact along one direction. In a recent development, Liu et al. (2019) successfully constructed a triaxial Hopkinson bar and investigated the dynamic behavior of sandstone specimens under combined static true triaxial confinement and dynamic loading from a single direction.

However, none of the existing SHPB systems are capable of conducting dynamic tests under true triaxial impact conditions. In fact, rocks and rock-like materials may encounter complex multi-axial and multi-directional impacts, which can be either synchronous or asynchronous, with equal or unequal magnitudes in different directions. For instance, during shaft excavation and mining operations employing the drill-and-blast method, rocks situated near the center of spirally arranged boreholes are often subjected to multidirectional blasting waves (e.g., symmetric, biaxial/four-directional, or triaxial/six-directional) that arrive at different times and exhibit directional variability. Similarly, in scenarios involving ballistic impact and penetration, protective rock and concrete structures are exposed to multiaxial dynamic loading (Karinski et al. 2017; Luo et al. 2019). Therefore, it is essential to develop an advanced dynamic testing system capable of applying controlled true triaxial impacts to rock specimens under laboratory conditions.

This study introduces the development of a dynamic true triaxial electromagnetic Hopkinson bar (DTEHB) system, an innovative experimental platform for investigating rock dynamic behaviors subjected to coupled three-dimensional (3D) dynamic disturbances and in-situ static stresses, with strain rates between 10^1 s^{-1} and 10^3 s^{-1}. The fundamental working principles and the structural configurations of the system are introduced in detail, as well as the key technical challenges

experienced during its development. The experimental validation confirms that the system is reliable and effective in simulating the conditions of true triaxial dynamic loading. The DTEHB system has been developed and implemented in this manuscript to thoroughly understanding of three-dimensional rock dynamics and facilitates further applications in geotechnical engineering.

2. State-of-the-Art of Split Hopkinson Bar

A conventional SHPB system consists of four main components: a striker, an incident bar, a transmitted bar, and a buffer bar. During testing, the test specimen is first placed between the incident and transmitted bars, and then a striker was driven by high pressure gas to impact the free end of the incident bar. A longitudinal stress wave is then generated and propagates along the incident bar. When the stress wave reaches to the bar-specimen interface, a part of the incident stress wave is reflected at the contact surface between the incident bar and specimen (reflected wave). And the wave propagates through the specimen, forming a transmitted wave at the contact surface with the transmission bar. A pair of strain gauges was attached on the surfaces of the incident and transmitted bars to monitor the dynamic strain response of the bars. The average dynamic stress, strain, and strain rate histories of the specimen can be calculated based on one-dimensional elastic stress wave theory and the standard data reduction methodology recommended by the ISRM (Zhou et al. 2012).

Although the SHPB technique has been widely adopted for dynamic testing of various materials, it remains an approximation rather than an optimum solution due to several inherent limitations. Achieving dynamic stress equilibrium during SHPB testing is a basic assumption, which guarantees its internal uniform deformation (Chen and Song 2011; Kolsky 1963). Conversely, deviations from dynamic stress equilibrium may give rise to inertial stresses, which distort the amplitude of the transmitted wave recorded in the transmitted bar. In brittle materials, for example, rock and concrete, dynamic compression under non-equilibrium conditions may cause the premature failure at exceedingly low strains, significantly attenuating the transmitted wave pulse (Lindholm et al. 1974). In this regard, pulse shaping techniques have been developed to shape the conventional trapezoidal incident pulse into a half-sine wave with a gradual rise time, thereby promoting dynamic stress equilibrium within the testing specimen (Frew et al. 2002; Li et al. 2009; Song and Chen 2004). Nevertheless, achieving complete dynamic stress equilibrium is continue to a challenging goal, as the

incident pulse must propagate through the specimen to establish uniform stress distribution (Frew et al. 2002). Additionally, the deviation of conventional pneumatic launching systems and precise pulse may affect the profiles of the incident pulse under identical gas pressure conditions. This challenge lead to a lack of repeatability of stress wave and further complicates the interpretation of dynamic test results.

In conventional SHPB testing, the incident stress pulse is generated by mechanical methods, such as striker impact (Chen and Song 2011) or a pre-tensioned bar section suddenly releases (Cadoni et al. 2009). However, there are inevitably mechanical errors of these traditional methods, making it hard to generate multiple synchronized incident stress pulses, which is inability to achieve multi-axial and multi-directional dynamic testing. As a consequence, most existing SHPB systems are restricted to uniaxial dynamic loading. A notable advancement was reported by Nie et al. (2018b), who developed a symmetrically loaded SHPB apparatus utilizing electromagnetic energy conversion, enabling synchronous bidirectional compression or tension testing.

The majority of so-called triaxial SHPB systems can only apply axisymmetric triaxial confinement ($\sigma_1 \geqslant \sigma_2 = \sigma_3 \neq 0$) to test specimens (Chen and Song 2011; Frew et al. 2002; Gran et al. 1989; Gary and Bailly 1998; Hokka et al. 2016; Li et al. 2008; Nemat-Nasser et al. 2000; Yuan et al. 2011; Peng et al. 2019). A key exception is the true triaxial compressed SHPB proposed by Zhao and Cadoni (2009) and further developed at Monash University (Zhao et al., 2015; Liu et al., 2019), which can apply independent triaxial static confining pressures. Furthermore, as underground engineering ventures into greater depths, rocks are increasingly subjected to thermo-mechanical coupling effects. However, no existing laboratory apparatus has been developed to study the coupled effects of real-time thermal treatment and dynamic and static triaxial stresses.

It is therefore essential to develop an innovative 3D dynamic testing device that is capable of repeatably generating stress waves with precise waveform control, accurately synchronizing multi-directional stress wave arrival times, and simulating the coupled effects of true triaxial synchronous impacts and *in situ* static stresses. Such an advancement would overcome the current constraints of SHPB technology and provide new insights into the dynamic behavior of rocks under complex loading environments.

3. Design and Configuration of the DTEHB System

Considering the inherent limitations of conventional SHPB systems, and to overcome critical challenges in analyzing three-dimensional dynamic responses and failure mechanisms in underground rock engineering structures during construction and operation, this study presents an innovative development of the DTEHB system. The developed brand-new testing system meets true triaxial dynamic loading with high-precision control, adjustable loading parameters, and repeatable stress waveforms. As illustrated in Fig. 1, the DTEHB system has four main components: a main control system of the dynamic true triaxial Hopkinson bar, a triaxial/six-directional electromagnetic stress pulse synchronous loading system, a triaxial/six-directional static-dynamic coupling loading system, and a multivariate dynamic real-time data acquisition and analysis system. This proposed system promotes to thoroughly investigate the dynamic mechanical behavior and failure mechanisms on brittle materials (including rocks, hard soils, concrete, ceramics, composites, polymers, energy-absorbing materials, and aerospace materials) under complex loading conditions. The system provides a wide range of dynamic impact loadings, ranging from symmetric loading to biaxial/four-directional and triaxial/six-directional loading, while accounting for in-situ stress conditions.

3.1 Principle of the DTEHB

Figure 2 presents the schematic of the stress state and wave propagation within the triaxial bar system. The specimen is subjected to a combined loading condition comprising static true triaxial confining pressures ($\sigma_x \neq \sigma_y \neq \sigma_z \neq 0$) and dynamic true triaxial impact loading. Notably, the static triaxial confining stresses are applied to the specimen before applying dynamic true triaxial impacts. As depicted in Fig. 2, the stress waves generated during the true triaxial impact test (i.e., $\varepsilon_{x\text{-}inc}$, $\varepsilon_{y\text{-}inc}$ and $\varepsilon_{z\text{-}inc}$) propagate synchronously and symmetrically along the corresponding bars and through the specimen. Under synchronous and symmetrical six-directional impact loading, three distinct stress waves (reflected waves, transmitted waves, and elastic waves induced by Poisson's effect) are generated along each principal axis. Although these three waves superimpose to form a single resultant wave, the one-dimensional elastic wave propagation theory is still followed in each axial direction (Cadoni and Albertini 2011). Moreover, the symmetric loading of two identical stress waves ensures the stress at both ends could achieve dynamic equilibrium rapidly along the loading direction

during impact. Consequently, the one-dimensional elastic wave propagation theory remains applicable for interpreting the dynamic response of the specimen under true triaxial impact loading.

To further clarify wave propagation in the DTEHB system, Fig. 3 presents an *x*-*t* diagram depicting wave propagation along the *x*-axis under symmetric loading conditions. Two identical incident waves propagate simultaneously and symmetrically from the ends of the right and left incident bars toward the specimen. Herein, the incident waves originating from the right and left bars are defined as ε_{inc_right} and ε_{inc_left}, respectively. In general, when a stress wave encounters the bar-specimen interface, a portion transmits through the specimen into the output bar, while the remaining portion reflects back into the input bar. As shown in Fig. 3, upon reaching the right bar-specimen interface, the right-propagating wave partially reflects while the transmitted component propagates through the specimen into the left input bar. Similarly, the left-propagating wave follows an analogous transmission-reflection mechanism. Given that the wave transit time through the specimen is negligible compared to the incident wave duration, the initial wave arriving at the right input bar represents a superposition of the reflected component from the right incident wave and the transmitted component from the left incident wave, denoted as ε_{ref_right}. An analogous superposition occurs in the left input bar, yielding ε_{ref_left}.

To avoid superposition of the incident and reflected waves in each bar, the two pulses are recorded by the resistance strain gauges mounted at midpoints of the bars. Since the square bars exhibit slenderness and the incident waveform approximates a half-sine pulse with minimal high-frequency content, waveform dispersion and oscillations are considered negligible. Therefore, in accordance with one-dimensional stress wave theory (Kolsky 1963), the dynamic forces (P) and particle velocities (V) at the right and left ends of the specimen can be calculated as follows:

$$P_{left} = AE(\varepsilon_{inc\_left} + \varepsilon_{ref\_left}),\ P_{right} = AE(\varepsilon_{inc\_right} + \varepsilon_{ref\_right}) \tag{1}$$

$$V_{left} = C(\varepsilon_{inc\_left} - \varepsilon_{ref\_left}),\ V_{right} = C(-\varepsilon_{inc\_right} + \varepsilon_{ref\_right}) \tag{2}$$

where C, A and E are the P-wave velocity, cross-section area and elastic modulus of the input bar, respectively.

Under symmetric loading conditions with identical incident waves from both the right and left sides, dynamic stress equilibrium can be effectively maintained throughout the loading process. Consequently, the dynamic stress within the specimen can be represented by the average stress

measured on its two boundaries. In accordance with one-dimensional stress wave theory (Kolsky 1963), the dynamic stress $\sigma(t)$, strain rate $\dot{\varepsilon}(t)$ and dynamic strain $\varepsilon(t)$ of the specimen under dynamic impact loading along each axial direction can be computed as follows (Nie et al. 2018b; Xie et al. 2021):

$$\sigma(t)=\frac{\sigma_{left}+\sigma_{right}}{2}=\frac{1}{2}\frac{A}{A_s}E(\varepsilon_{inc\_left}+\varepsilon_{inc\_right}+\varepsilon_{ref\_left}+\varepsilon_{ref\_right}) \tag{3}$$

$$\dot{\varepsilon}(t)=\frac{V_{left}-V_{right}}{L_s}=\frac{C}{L_s}(\varepsilon_{inc\_left}+\varepsilon_{inc\_right}-\varepsilon_{ref\_left}-\varepsilon_{ref\_right}) \tag{4}$$

$$\varepsilon(t)=\int_0^t\dot{\varepsilon}dt=\frac{C}{L_s}\int_0^t(\varepsilon_{inc\_left}+\varepsilon_{inc\_right}-\varepsilon_{ref\_left}-\varepsilon_{ref\_right})dt \tag{5}$$

where L_s and A_s are the length and cross-section area of the specimen, respectively.

The strength of rock and rock-like materials exhibits a significant increase with elevated confining pressure (Patton et al. 1998; Richter et al. 2018; Wasantha and Ranjith 2014; Zhu et al. 2016). Moreover, under high confining pressure conditions, brittle failure transitions to ductile deformation (Kumari et al. 2017; Peng et al. 2015; Scott and Nielsen 1991). Given these mechanical responses, the von Mises stress criterion may be adopted to evaluate the dynamic deformation and failure behavior of specimens subjected to coupled dynamic true triaxial impacts and static triaxial stresses. The equivalent stress ($\bar{\sigma}$) and equivalent strain ($\bar{\varepsilon}$) of the specimen under the combined influence of triaxial static pressures and dynamic true triaxial impacts can be calculated as follows (Xu et al. 2020):

$$\bar{\sigma}=\sqrt{\frac{1}{2}[(\sigma_{x\_dyn}+\sigma_{x\_static}-\sigma_{y\_dyn}-\sigma_{y\_static})^2+(\sigma_{y\_dyn}+\sigma_{y\_static}-\sigma_{z\_dyn}-\sigma_{z\_static})^2+(\sigma_{z\_dyn}+\sigma_{z\_static}-\sigma_{x\_dyn}-\sigma_{x\_static})^2]} \tag{6}$$

$$\bar{\varepsilon}=\sqrt{\frac{2}{9}[(\varepsilon_{x\_dyn}+\varepsilon_{x\_static}-\varepsilon_{y\_dyn}-\varepsilon_{y\_static})^2+(\varepsilon_{y\_dyn}+\varepsilon_{y\_static}-\varepsilon_{z\_dyn}-\varepsilon_{z\_static})^2+(\varepsilon_{z\_dyn}+\varepsilon_{z\_static}-\varepsilon_{x\_dyn}-\varepsilon_{x\_static})^2]} \tag{7}$$

where σ_{i_dyn}, σ_{i_static}, ε_{i_dyn} and ε_{i_static} represent dynamic stress, static confining pressure, dynamic strain and static strain corresponding to the peak static confining pressure along the *i*-axis (*i*=*x*, *y*, and *z*).

3.2 Configuration of the DTEHB

As aforementioned, the DTEHB is able to realize multi-axial and multi-directional synchronous

or asynchronous loading (e.g., from 1D symmetric loading to biaxial/four-directional and triaxial/six-directional loading), dynamic-static coupled loading, controllable and repeatable dynamic impact. As illustrated in Fig. 1, the DTEHB consists of a main control system of the dynamic true triaxial Hopkinson bar, a triaxial/six-directional electromagnetic stress pulse synchronous loading system, a triaxial/six-directional static-dynamic coupling loading system, and a multivariate dynamic real-time data acquisition and analysis system.

The main control system of the dynamic true triaxial Hopkinson bar comprises three components: the primary structural frame of the triaxial Hopkinson bar, a 3D alignment and leveling device for precise triaxial Hopkinson bars and specimen positioning, and an energy-absorbing buffer with self-resetting capability. The benchmark platform provides support and reference plane for the whole system. The primary structural frame is a 3D symmetric frame structure with sufficiently high stiffness. To achieve true triaxial loading, the Hopkinson bar is designed with a square cross-section. In the DTEHB, three pairs of orthogonal square bars with circular bulges constitute the 3D dynamic impact loading bar system, as shown in Fig. 2. There are three key components of the 3D centering and leveling system, as shown in Fig. 1(b): the benchmark box, which is the reference datum for the alignment of the triaxial Hopkinson bars; the 3D adjustment and support device for Hopkinson bars, which allows for precise control angular of each square bar; and the pitch adjustment device of the electromagnetic stress pulse generator, which ensures optimal alignment and leveling of the bar with the pulse generator. Therefore, the specimen, Hopkinson bars, and pulse generators are precisely coaxially aligned under coordinated operation, achieving reliable and repeatable experimental results under dynamic true triaxial loading conditions. The energy-absorbing buffer with a self-resetting mechanism is designed to minimize the gap between the Hopkinson bar and the electromagnetic stress pulse generator and to effectively absorb the reaction energy after dynamic impact loading. A detailed description of the energy-absorption buffer and self-resetting device is provided in Section 4.2.3.

The triaxial/six-directional electromagnetic stress pulse synchronous loading system includes two main parts: an electromagnetic stress pulse generation system and a triaxial/six-directional electromagnetic stress pulse synchronized control system (SCS). In this system, electrical energy is converted into electromagnetic pulses via the cooperation of electromagnetic stress pulse generators (ESPGs) and the SCS, the generated stress waves propagate along the elastic bars and apply to the tested specimen. The pulse duration and amplitude can be precisely controlled by adjusting the

capacitor group and charging voltage of the ESPGs. Additionally, the high-precision SCS ensures precise discharge timing to generate the electromagnetic stress pulses across multiple ESPGs, thereby enabling multi-axial and multi-directional synchronous dynamic loading in several loading configurations (uniaxial symmetric loading, biaxial/four-directional loading, and triaxial/six-directional loading), in either synchronous or asynchronous mode.

The triaxial/six-directional static-dynamic coupling loading system generally includes a hydraulic servo-controlled confining pressure loading subsystem, a confining pressure loading apparatus, and a triaxial bar assembly with circular bumps. The true triaxial static stresses were applied to specimen by the hydraulic servo-controlled technology of the confining pressure loading subsystem, allowing independently and identically or varying magnitudes of each principal stress component, thereby accurately replicating in situ static stress conditions. One advantage of the servo-controlled system is that the true triaxial static confining pressure could be maintained at a near-constant level during testing, thereby the pressure oscillations that would otherwise arise due to the Poisson effect under dynamic loading could be effectively mitigated. The stress on the specimen ensured stability.

Accurate acquisition and analysis of experimental data are critical in dynamic testing, as the validity of results hinges on the precise capture and isolation of true specimen responses from surrounding noise. Reliable measurements of dynamic mechanical characteristics, such as strain signals, acoustic emissions, and development of fractures, help to understanding dynamic behaviors of rock. The DTEHB meets these requirements through the multiple advanced techniques, including both contact and non-contact measurements, real-time monitoring, post-test analysis, and macro- to micro-scale characterization using both nondestructive and destructive approaches. Altogether, they provide a comprehensive analysis of the dynamic rock responses. Table 1 lists the function of the instrumentation and techniques in the DTEHB for data acquisition and analysis. Notably, digital image correlation and ultra-high-speed imaging are utilized to capture surface deformation and fracture dynamics under the loading conditions of uniaxial symmetric and biaxial/four-directional dynamic loading. However, in the true triaxial dynamic loading tests, the specimen is fully confined by six opaque bars, and there is no free surface allow to the direct visual access, resulting in these optical techniques being unapplicable.

4 Technical Challenges Overcome in the Development of the DTEHB

To realize the functions of the DTEHB, several critical technical challenges have been resolved, including the following: High precision in generating stress wave: a novel technique has been developed to produce stress waves with exceptional accuracy and repeatability. Synchronous multidirectional wave generation: an innovative methodology allows the synchronous generation of multiple identical stress waves with high consistency. Precision-controlled multidirectional loading: a specialized technique enables the precise synchronization of stress wave loading from different axes, maintaining an arrival time error within the microsecond range. Dynamic true triaxial impact coordination: an effective control system has been designed to coordinate the process of dynamic triaxial impact loading. Servo-controlled static pressure loading: a servo-controlled triaxial static pressure loading system has been developed to apply in situ stresses.

4.1 Triaxial/Six-directional Electromagnetic Stress Pulse Synchronous Loading System

As previously mentioned, conventional SHPB systems exhibit an inherent limitation in generating high-precision and repeatable dynamic pulses, making it difficult to conduct multi-axial and multi-directional dynamic loading tests under either synchronous or asynchronous conditions. This limitation primarily arises from the striker impacts or the sudden release of pre-tensioned bar sections in traditional mechanical loading methods, which face technical challenges in achieving microsecond-scale synchronization and generating controllable incident stress pulses with sufficient precision and repeatability (Nie et al. 2018a; Cadoni and Albertini 2011). Therefore, this study employs an innovative technique based on the electromagnetic energy conversion principle, it allows the system to generate multiple identical and synchronized stress waves with high precision and repeatability. The synchronized control system (SCS) ensures precise temporal coordination between stress wave generation and the application of dynamic loading. Moreover, an automatic control system manages the electromagnetic pulse generation mechanism, ensuring operational accuracy and safety. The integration of these key components—electromagnetic energy conversion, SCS, and the automatic control system—achieves controllable, realistic true triaxial dynamic loading conditions, thereby addressing a critical gap in rock mechanics experiments.

4.1.1 Electromagnetic Stress Pulse Generation Device

The DTEHB consists of three orthogonally arranged electromagnetic split Hopkinson bar assemblies, as demonstrated in Fig. 1. Given that the structural configuration, operational principles, and loading mechanisms are identical along all three axes (X, Y, and Z), and each axis operates independently without mutual interference, therefore, the following discussion focuses on the design and functionality of the system along a single axis for brevity.

As shown in Fig. 4, the single-axis bar system consists of two ESPGs with active and inductive coils, two incident bars, and two symmetrically positioned charging circuits. In each charging circuit, a thyristor is used to control the discharge. A bridge rectifier and a high-power transformer are employed to convert an alternating voltage input (380 V) into a high-voltage direct current (DC). A bank of series or parallel configured pulse capacitors serves as an energy storage unit during charging. Each charging circuit connects to its corresponding active coil of the ESPG and forms an LC oscillation circuit. Once triggered, the thyristors are turned on at once, the fully charged capacitor banks allow the discharge current to flow equally into both active coils. Each thyristor operates as a unidirectional switch, hence, only the forward discharge current propagates while the reverse current is blocked. Subsequently, the pulsed current flowing through the coils is converted to a mechanical stress wave by electromagnetic induction. A detailed theoretical treatment of the electromagnetic conversion process can refer to Nie et al. (2018a) for further information.

Attainable repeatability and precision of the electromagnetic stress pulses depend on the meticulously design and fabricate of the ESPG, especially its active coil. Fig. 5 shows an exemplified structural and parametric design for an active coil. An outer diameter of the active coil is144 mm and a height of 58 mm, with its core made from a 4-mm-thick and 15-mm-high copper strip wound in eight concentric layers in a Swiss roll configuration. For machining accuracy and inductance consistency, the copper strips are cut precisely using wire electrical discharge machining. This provides the unit a clear 2-mm inter-turn gap, which is filled with insulating rubber to prevent interlayer discharge between copper strips. Additionally, a high-strength composite base is incorporated to bear the reaction forces that acting perpendicular to the coil. Two protruding copper strips serve as the positive and negative electrodes, and an insulating block is interposed to avoid short-circuiting.

Upon fabrication, the inductance of the ESPG is determined, as it is inherently governed by the number of copper strip turns and remains fixed for a given generator (Nie et al., 2018a). Based on underdamped LRC circuit theory, the discharge current duration is primarily dictated by the active coil's capacitance and can be estimated as follows:

$$T = \pi\sqrt{LC_e} \tag{8}$$

where L is the inductance of the active coil, and C_e is the and capacitance of the active coil.

Based on the principle of electromagnetic conversion, a time-dependent Lorentz force is induced at the surface of the adjacent inductive coil during the discharge current flowing into the active coil, thereby generating a stress pulse. The duration of this stress pulse is linked to the transient duration of the discharge current, which is primarily determined by the capacitance of the discharge current. By modifying the capacitance through the addition or removal of parallel or series-connected capacitors, the ESPG generates a series of stress pulses with different durations.

Fundamentally, the capacitor discharge in an LC circuit released the energy, which is converted into the energy of the stress pulse by electromagnetic transduction. Thus, the amplitude of the electromagnetic stress pulse can be precisely controlled by adjusting the stored energy of the capacitor during the charging and discharging. According to LC circuit discharge theory, the electrical energy stored in the capacitor can be expressed as:

$$W_e = \frac{1}{2}C_e U^2 \tag{9}$$

where U is the charging voltage.

The pulse duration is modulated by the capacitor group, a desired pulse can be obtained by precisely adjusting the charging voltage of LC circuit. This mechanism enables effective control over the pulse amplitude. Considering the requirements of rock dynamic tests, the wave amplitude is designed to fall within the range of 0 to 600 MPa, as well as the wave duration is set to a range of 300 to 800 μs.

4.1.2 Synchronous Pulse Control System

As aforementioned, the true triaxial dynamic testing apparatus consists of three orthogonally arranged symmetric Hopkinson bars, and each Hopkinson bar is subjected to the independently generated electromagnetic stress pulses. The achievement of true triaxial dynamic impact loading

requires generating incident stress pulses synchronously along all three axes. Accordingly, the primary technical challenge is to precisely control and synchronize these stress pulses.

Fig. 6 illustrates the schematic of the synchronous control system. There is a transformer and a bridge rectifier in the charging circuit, which is similar to that of a conventional uniaxial symmetric electromagnetic Hopkinson bar (SHB) system. Six parallel-connected capacitors are integrated into this circuit, each controlled by an independent switch. Therefore, the key challenge is to provide an independent trigger signal for the thyristor on each axis. In order to achieve this demand, a digital delay generator (DG645) with nanosecond-level timing accuracy coordinating to work together with a multichannel high-voltage pulse trigger are adopted for the SCS. The above methods can make sure the precise control of the stress pulse initiation time along the three loading directions with a synchronization accuracy within 5 μs which is a critical requirement for realizing true triaxial impact loading.

During the testing process, when the pre-selected capacitor reaches the target charge, the digital delay generator immediately outputs a trigger signal to the multichannel high-voltage pulse trigger at the scheduled time. The trigger then simultaneously activates the thyristors in the designated branches, and the resulting discharge current provides energy to the ESPGs. Through electromagnetic conversion, synchronized stress pulses are generated. To further improve synchronization accuracy, an energy-absorbing buffer with self-resetting capability was developed. The above device can effectively reduce the gap between the electromagnetic stress pulse generator and the Hopkinson bar, which ensures their precise contact alignment. This mechanism minimizes mechanical delays, thereby enhancing overall synchronization accuracy. Ultimately, the generated stress pulses propagate into the Hopkinson bars as incident waves, as shown in Fig. 2.

The synchronous discharge control system ensures the precise generation of electromagnetic stress pulses with high-time coordination. When integrated with the self-resetting, energy-absorbing buffer of the dynamic loading system, it can achieve multiaxial and multidirectional synchronized impact loading with a timing error of less than 5 μs.

4.1.3 Central Control System

The synchronization of the dynamic triaxial impact loading system requires a control system with precise operation. As illustrated in Fig. 7, the control system can be divided into three primary

modules: the human-machine interface (HMI) system, the charging and discharging system, and the dynamic testing system. During operation, the HMI system monitors the real-time system status of system and converts manual inputs into digital control signals. These signals are subsequently output to the charging and discharging system for controlling the charging or discharging of the capacitor bank. During this process, the stored electrical energy is converted into electromagnetic energy in the dynamic testing system as it discharges, the incident stress waves are generated and then applied to the specimen and characterize its dynamic response.

In the DTEHB system, the charging and discharging system is a key component. Upon the HMI system issues a charging command, the programmable logic controller (PLC) activates the charging circuit and connects it to the capacitor bank. At the same time, voltage and current sesors continuously monitor electrical parameters and convert them into analog signals, which the PLC monitors in real-time through analog I/O modules. To ensure operational safety, the system integrates emergency monitoring mechanism, for example, if overcharging or an excessively high charging rate is detected, the PLC immediately stops charging. Upon receiving a discharging command, the PLC connects the discharge circuit and releases the energy stored in the capacitor bank through the ESPGs, thereby powering the dynamic testing system. In emergency situations, the PLC can bypass normal operations and safely release stored energy through a ground leakage triggering device, preventing potential damage to the system.

4.2Triaxial/Six-directional Static-Dynamic Coupling Loading System

In the conventional axisymmetric triaxial confined SHPB device, the applied static confining stress condition ($\sigma_1 \geqslant \sigma_2 = \sigma_3 \neq 0$) differs from the true in-situ stress state ($\sigma_1 \geqslant \sigma_2 \geqslant \sigma_3 \neq 0$). To address this limitation, a servo-controlled static triaxial loading system has been developed. This system integrates a high-stiffness triaxial loading frame with a servo-controlled hydraulic pressure loading system. A critical requirement is that the servo-control system is able to ensure minimal fluctuation of the static confining pressure during dynamic loading. Furthermore, a dynamic-static coupling loading conversion control device has been designed to achieve seamless coupling between static and dynamic triaxial loading. Additionally, considering the requirements of efficient energy absorption and high repeatability of electromagnetic stress pulses, an energy absorption buffer with self-resetting capability has been incorporated into the system.

4.2.1 Servo-controlled static triaxial pressure loading device

As illustrated in Fig. 1, the loading frame consists of an orthogonal triaxial loading system. The supporting frame is made of 42CrMo high-strength alloy steel with precision machining, as it exhibits exceptional rigidity and mechanical strength. This triaxial frame bears the entire weight of the system and provides an excellent reference plane to apply accurate loads on the specimen.

The servo-controlled hydraulic pressure system consists of a hydraulic pump station, three independent hydraulic cylinders, and a servo control unit. The system is designed for a maximum confining pressure of 300 MPa, with an accuracy of ±0.5 MPa. Fig. 8 shows the schematic diagram of the static confining pressure applied along one principal axis. The hydraulic loading assembly for each axis contains a hydraulic cylinder, a reference benchmark box, support frames, two confining pressure loading frames, and two square transmission bars.

4.2.2 Static-dynamic coupling loading conversion device

There are six square bars in system, each one with a size of 50 × 50 × 2800 mm^3. To minimize the effects of electromagnetic interference in strain signals, the square bar is made of anti-magnetic titanium alloy with a yield strength of approximately 1050 MPa. Additionally, considering the stress wave dispersion and oscillation, the square bars are precision-machined with a maximum straightness deviation of 0.1‰ and a surface polishing flatness of 0.8. Since the incident end of the square bar interfaces directly with the ESPG—which cannot sustain prestress—applying static confining pressure directly at this end is infeasible. To overcome this limitation, a circular bulge (Ø90 mm, thickness 70 mm) is integrated into the bar at a distance of 150 mm from the incident end, as shown in Fig. 8. This design allows the static confining pressure to be applied through the bulge rather than the bar's incident end. The static confining pressure is applied by a servo-controlled hydraulic system (Fig. 8). The static confinement is applied on the bulge of the bar and then transmitted to the specimen through the adjacent bar segments.

Except the confining pressure loading frame and square bar, all structural components, are fixed within a rigid unified frame. During operation, the specimen is sandwiched between two square bars, with one end of the frame (right side in Fig. 8) fixed and the other end serving as the confining pressure loading end. The hydraulic pump station drives the piston inside the hydraulic cylinder, moving the loading frame until it contacts the circular bulge. As the piston moves to the right, the

loading frame transfers the axial load to the specimen through the bulge and the adjacent square bar. The key point is that the right-side frame ensures that the right square bar and specimen face remain stationary throughout the loading process. Once the target confining pressure is reached, this pressure is maintained constant for subsequent dynamic impact testing. During dynamic loading, the static confining pressure remains relatively stable to prevent fluctuations caused by the Poisson effect, ensuring consistent boundary conditions.

4.2.3 Energy absorption buffer with self-resetting capability

During the testing process, there may be an initial gap between the bar and the ESPG, which can lead to the mechanical delay resulting the deterioration of multi-axial wave consistency and distortion of the stress waveform. In addition, under dynamic loading, part of the incident energy remains in the bar and propagates into the ESPG even the system frame, which may affect the structural integrity and long-term durability of the testing device. In order to alleviate the above problems, a stress pulse energy absorption buffer with self-resetting capability has been developed.

As shown in Fig. 9, the buffer consists of two compressible/extendable hydraulic cylinders and two large-capacity nitrogen springs (load capacity: 600 MPa). These components work together to absorb the residual energy transmitted by the bars, thereby protecting the testing system during dynamic loading. Notably, by increasing air pressure, the hydraulic cylinders can be extended, effectively eliminating the initial gap and ensuring waveform consistency in the incident stress pulse. Additionally, maintaining constant air pressure allows the hydraulic cylinders to retract to their original position after each test, enabling automatic reset for repeated experiments. To further enhance system stability, linear guides have been integrated below the ESPG to ensure precise linear displacement and prevent fluctuations caused by the lateral movement of the ESPG.

5 Verification and Testing

To validate the functionality and performance indicators of the developed DTEHB system, a series of experimental verification tests were conducted.

5.1 Adjustability of stress wave duration

Fig. 10 shows incident stress waves of different durations generated by the ESPG. By adjusting

the capacitance of the capacitor bank—for example, increasing it from 1 mF to 4 mF—the pulse duration of the incident stress wave can be controlled within a range of 400 to 800 μs. Notably, the stored energy in the capacitor bank is determined by both the charging voltage and capacitance, as shown in Eq. (9). Therefore, to maintain a consistent wave amplitude while varying pulse durations under different capacitances, the charging voltage must be adjusted accordingly.

Additionally, it can be found that the stress wave duration can be reduced to approximately 300 μs in Fig. 10 by means of decreasing the number of copper strip turns from 16 to 8. This occurs because the number of turns is directly proportional to the inductance of the active coil. Cutting down the number of turns decreases the coil inductance, resulting in a decrease in the stress wave duration. Conversely, increasing the number of turns prolongs the wave duration due to the resultant increase in inductance.

5.2 Adjustability of stress wave amplitude

Fig. 11a presents the stress wave amplitude various with different charging voltages when the capacitance is maintained at 4 mF. With the increasing of the charging voltage from 1500 V to 4000 V, the stress wave amplitude correspondingly achieves an ascent from from 100 MPa to 600 MPa, while the wave duration keeps at about 725 μs. This illustrates that the stress wave amplitude can be precisely adjusted to achieve the requirements of different experimental conditions. In addition, the stress wave amplitude is also related to the capacitance and the number of turns in the active coil (Fig. 11b), which can be utilized as the basis for the its adjusting. Therefore, by systematically adjusting the capacitance, charging voltage, and configuration of the active coil, the desired stress wave duration and amplitude can be precisely tailored to achieve specific testing requirements.

5.3 Repeatability of stress waves

The reproducibility and reliability of experimental results critically depend on the repeatability of incident stress waves. Fig. 12 presents the results of repeated incident stress wave generation using the same ESPG (with an active coil capacitance group of 2 mF and 12 turns of copper tape) at two different charging voltages (1500 V and 2000 V). It occurred that over the electromagnetic conversion principle, the generated incident stress waves achieve excellent repeatability (≥99%) in terms of wave amplitude, waveform shape, and duration. These findings confirm that electromagnetic

conversion technology provides a robust solution for generating highly repeatable incident stress waves, overcoming the limitations associated with traditional mechanical impact methods that rely on striker-bar collisions at the incident bar end.

5.4 Static true triaxial confining pressures

As aforementioned, the dynamic true triaxial Hopkinson bar is able to to accurately apply independent triaxial static confining pressures to specimen, which is crucial for investigating the mechanical behavior of deep underground rocks under coupled true triaxial static confinement and dynamic disturbances. In Fig. 13, the static true triaxial confining pressure loading system successfully imposes static stresses along the X, Y, and Z axes smoothly and independently, and there is no cross-interference between axes. The results confirm that the DTEHB system can maintain stable confining pressure upon reaching the preset load, proving its effectiveness to simulate true triaxial static stress conditions.

5.5 Dynamic true triaxial loading test

To verify the viability and effectiveness of the DTEHB, dynamic true triaxial loading tests were carried out on cubic coal and sandstone specimens, respectively. It should be noted that under dynamic true triaxial impact loading, volumetric compression inevitably occurs due to the compaction and collapse of pre-existing defects within the rock. Consequently, if the specimen dimensions match the cross-sectional side length of the square bars (50 mm), bar collision becomes unavoidable. To address this issue, and given that the dynamic deformation of brittle rocks typically remains below 1%, the specimen side length was designed to increase 1 mm, this ensures sufficient deformation space (up to 2% strain) and also prevents bar interference. Additionally, a 0.5 mm chamfer was made at each edge of the cubic specimen to minimize geometric mismatch between the specimen and the loading surfaces.

Fig. 14 demonstrates the typical results of a dynamic true triaxial impact test on a coal specimen. Fig. 14a shows the incident and reflected voltage signals recorded on three orthogonal sets of titanium alloy bars. The results demonstrate that the six independent ESPGs produce highly synchronized incident stress waves, with arrival time discrepancies of less than 5 μs and near-identical waveforms and pulse durations. The amplitude of the six incident waves exhibits remarkable consistency (>99%),

the Z1 amplitude being only 1.89% higher due to a marginally greater discharge voltage (~10 V) in its corresponding capacitor. The above indicate that the DTEHB system can generate consistently synchronized multiaxial stress pulses, thereby achieving uniform dynamic loading. The reflected waveforms are generally consistent, but the peaks are more variable due to the anisotropic wave transmission and reflection properties of the rock.

Fig. 14b shows the dynamic stress equilibrium at both ends of the specimen along the X-, Y-, and Z-axes, it was calculated by the stress waves in Fig. 13a. In general, the stress difference between opposing specimen faces remains below 5%, which can be regarded as achieving dynamic stress equilibrium. The results indicate that the dynamic stress equilibrium was achieved well, and equilibrium time accounting for 63–82% of the total stress wave duration in each direction. This effectively resolves the inherent limitations in stress equilibrium for the conventional SHPB systems.

Fig. 14c depicts the dynamic stress-strain responses along the three principal axes. The curves exhibit similar evolutionary trends: an initial compaction phase followed by linear elastic deformation, a brief nonlinear regime, peak stress attainment, and post-peak rebound unloading. Despite nearly identical incident stresses in all directions (Fig. 13a), slight variations in peak stresses arise due to material heterogeneity. Notably, the peak strain in the Z direction is larger than that in the X and Y directions, predominantly attributable to the presence of anisotropy in the specimen, which gives rise to a comparatively larger strain in the Z direction.

6 Summary

This paper presents the development of a novel dynamic true triaxial electromagnetic Hopkinson bar (DTEHB) system, designed to investigate the dynamic behavior of rocks under coupled multiaxial static and dynamic loading conditions. The system comprises a main control system of the dynamic true triaxial Hopkinson bar, a triaxial/six-directional electromagnetic stress pulse synchronous loading system, a triaxial/six-directional static-dynamic coupling loading system, and a multivariate dynamic real-time data acquisition and analysis system. The servo-controlled static triaxial confining pressure system enables independent application of true triaxial static stresses along three orthogonal directions. Electromagnetic energy conversion is employed to generate highly repeatable and precise stress pulses, while a synchronization control technique ensures that the time delay between multiple incident stress waves arriving at the specimen's loaded end face does not exceed 5 μs. The integrated

control system coordinates the dynamic triaxial impact loading process while ensuring both operational safety and optimal performance of the DTEHB. According to the electromagnetic energy conversion principle and the synchronous control techniques, the DTEHB system realizes the high-precision true triaxial synchronous impact loading. Moreover, the DTEHB system is capable of simulating coupled triaxial/six-directional impact and static confining pressure loading to replicate 3D in situ stress conditions, which is beyond the capability of conventional SHPB apparatus.

The development of the DTEHB system provides a cutting-edge dynamic testing platform, which enables the systematic study of dynamic behavior of rocks and other materials under 3D dynamic disturbances, with strain rates ranging from 10^1 s^{-1} to 10^3 s^{-1}, while accounting for in situ stress conditions. The anticipated findings derived from this system are expected to advance the theoretical framework of 3D rock dynamics and support practical applications in rock engineering.

CRediT authorship contribution statement

Heping Xie: Writing - original draft, Conceptualization, Methodology, Investigation, Formal analysis, Funding acquisition. Jianbo Zhu: Methodology, Writing - review & editing, Investigation, Supervision, Funding acquisition. Yulong Li: Methodology, Writing - review & editing, Investigation, Supervision. Tao Zhou: Methodology, Writing - review & editing, Investigation, Supervision. Weiyue Bao: Methodology, Writing - review & editing, Investigation, Formal analysis. Shiwei Zhang: Methodology, Writing - review & editing, Formal analysis. Zhongbin Tang: Methodology, Writing - review & editing. Tao Suo: Methodology, Writing - review & editing. Xiaoyong Song: Methodology, Writing - review & editing. Jian Zhao: Methodology, Writing – review & editing.

Declaration of competing interest

The authors declare that they have no known competing financial interests or personal relationships that could have appeared to influence the work reported in this paper.

Acknowledgements

This research is financially supported by the Program for Guangdong Introducing Innovative and Entrepreneurial Teams (2019ZT08G315) and the National Natural Science Foundation of China (52325404).

Data availability

Data will be made available on request.

Supplementary material

A supplementary video is supplied for better understanding of the design, principle, function and some potential applications of the DTEHB, and can be found online at https://doi.org/10.6084/m9.figshare.11473737.v1.

References

Ahrens TJ, Rubin AM. Impact-induced tensional failure in rock. *J Geophys Res Planets*. 1993;98(E1):1185-1203.

Cadoni E, Albertini C. Modified Hopkinson bar technologies applied to the high strain rate rock tests. *Advances in Rock Dynamics and Applications*. edited by Y. X. Zhou, and J. Zhao, 2011:79-104.

Cadoni E, Meda A, Plizzari GA. Tensile behaviour of FRC under high strain-rate. *Mater Struct.* 2009; 42(9):1283-1294.

Chen WW, Ravichandran G. Dynamic compressive failure of a glass ceramic under lateral confinement. *J Mech Phys Solids*. 1997;45(8):1303-1328.

Chen WW, Song B. Split Hopkinson Kolsky bar: design, testing and applications. Springer Science and Business Media. 2011.

Doan ML, Gary G. Rock pulverization at high strain rate near the San Andreas fault. *Nat Geosci.* 2009;2(10): 709-712.

Fairhurst CE, Hudson JA. Draft ISRM suggested method for the complete stress-strain curve for intact rock in uniaxial compression. *Int J Rock Mech Min Sci.* 1999;36(3):279-289.

Frew DJ, Forrestal MJ, Chen W. A split Hopkinson pressure bar technique to determine compressive stress-strain data for rock materials. *Exp Mech.* 2001;41(1):40-46.

Frew DJ, Forrestal MJ, Chen W. Pulse shaping techniques for testing brittle materials with a split Hopkinson pressure bar. *Exp Mech.* 2002;42(1):93-106.

Gary G, Bailly P. Behaviour of quasi-brittle material at high strain rate. Experiment and modelling. *Eur J Mech A Solids*. 1998;17(3):403-420.

Gran JK, Florence AL, Colton JD. Dynamic triaxial tests of high-strength concrete. *J Eng Mech.* 1989;115(5):891-904.

Goldsmith W, Sackman JL, Ewerts C. Static and dynamic fracture strength of barre granite. *Int J Rock Mech Min Sci.* 1976;13(11):303-309.

Hokka M, Black J, Tkalich D, Fourmeau M, Kane A, Hoang NH, Li CC, Chen WW, Kuokkala VT. Effects of strain rate and confining pressure on the compressive behavior of Kuru granite. *Int J Impact Eng.* 2016;91:183-193.

Ju Y, Sudak L, Xie HP. Study on stress wave propagation in fractured rocks with fractal joint surfaces. *Int J Solids Struct.* 2007;44(13):4256-4271.

Karinski YS, Zhutovsky S, Feldgun VR, Yankelevsky DZ. The equation of state of unsaturated cementitious

composites–A new multiscale model. *Int J Solids Struct.* 2017;109:12-21.
Kolsky H. Stress waves in solids. Courier Corporation. 1963.
Kumar A. The effect of stress rate and temperature on the strength of basalt and granite. *Geophysics*. 1968;33(3): 501-510.
Kumari WGP, Ranjith PG, Perera MSA, Shao S, Chen BK, Lashin A, Arifi N Al, Rathnaweera TD. Mechanical behaviour of Australian Strathbogie uranite under in-situ stress and temperature conditions: An application to geothermal energy extraction. *Geothermics*, 2017;65:44-59.
Lambert DE, Ross CA. Strain rate effects on dynamic fracture and strength. *Int J Impact Eng.* 2000;24(10):985-998.
Li JC, Li NN, Li HB, Zhao J. An SHPB test study on wave propagation across rock masses with different contact area ratios of joint. *Int J Impact Eng.* 2017a;105:109-116.
Li XB, Lok TS, Zhao J. Dynamic characteristics of granite subjected to intermediate loading rate. *Rock Mech Rock Eng.* 2005; 381:21-39.
Li XB, Zhou T, Li DY. Dynamic strength and fracturing behavior of single-flawed prismatic marble specimens under impact loading with a Split-Hopkinson pressure bar. *Rock Mech Rock Eng.* 2017b;50(1):29-44.
Li XB, Zhou ZL, Hong L, Yin TB. Large diameter SHPB tests with a special shaped striker. ISRM News J. 2009; 12:76-79.
Li XB, Zhou ZL, Lok TS, Hong L, Yin TB. Innovative testing technique of rock subjected to coupled static and dynamic loads. *Int J Rock Mech Min Sci.* 2008; 45(5):739-748.
Lindholm US, Yeakley LM, Nagy A. The dynamic strength and fracture properties of dresser basalt. *Int J Rock Mech Min Sci.* 1974;115:181-191.
Liu K, Zhang QB, Wu G, Li JC, Zhao J. Dynamic mechanical and fracture behaviour of sandstone under multiaxial loads using a triaxial Hopkinson bar. *Rock Mech Rock Eng.* 2019;52(7):2175-2195.
Lu YB, Li QM, Ma GW. Numerical investigation of the dynamic compressive strength of rocks based on split Hopkinson pressure bar tests. *Int J Rock Mech Min Sci.* 2010;*5*4(7):829-838.
Luo W, Chau VT, Bažant ZP. Effect of high-rate dynamic comminution on penetration of projectiles of various velocities and impact angles into concrete. *Int J Fract.* 2019;216(2):211-221.
Melosh HJ, Ryan EV, Asphaug E. Dynamic fragmentation in impacts: Hydrocode simulation of laboratory impacts. *J Geophys Res Planets*. 1992;97(E9):14735-14759.
Nemat-Nasser S, Isaacs J, Rome J. Triaxial Hopkinson techniques. *Materials Park. OH: ASM International,* 2000:516-518.
Nie HL, Suo T, Wu BB, Li YL, Zhao H. A versatile split Hopkinson pressure bar using electromagnetic loading. *Int J Impact Eng.* 2018a;116:94-104.
Nie HL, Suo T, Shi XP, Liu HF, Li YL, Zhao H. Symmetric split Hopkinson compression and tension tests using synchronized electromagnetic stress pulse generators. *Int J Impact Eng.* 2018b;122:73-82.
Olsson WA. The compressive strength of tuff as a function of strain rate from 10^{-6} to 10^{3}/sec. *Int J Rock Mech Min Sci.* 1991;28(1):115-118.
Patton TL, Logan JM, Friedman M. Experimentally generated normal faults in single-layer and multilayer limestone specimens at confining pressure. *Tectonophysics*. 1998;295(1-2):53-77.
Peng K, Liu ZP, Zou QL, Zhang ZZ, Zhou JQ. Static and dynamic mechanical properties of granite from various burial depths. *Rock Mech Rock Eng.* 2019;52(10):3545-3566.
Peng RD, Ju Y, Wang JG, Xie HP, Gao F, Mao LT. Energy dissipation and release during coal failure under

conventional triaxial compression. *Rock Mech Rock Eng.* 2015;48(2):509-526.

Perkins RD, Green SJ, Friedman M. Uniaxial stress behavior of porphyritic tonalite at strain rates to 10^3/second. *Int J Rock Mech Min Sci.* 1970;75:527-535.

Qi CZ, Xia C, Li XZ, Sun YJ. Effect of inertia and crack propagation on dynamic strength of geologic-type materials. *Int J Impact Eng.* 2019;133:103367.

Ranjith PG, Zhao J, Ju M, De Silva RV, Rathnaweera TD, Bandara AK. Opportunities and challenges in deep mining: A brief review. *Engineering*. 2017;3(4):546-551.

Reddish DJ, Stace LR, Vanichkobchinda P, Whittles DN. Numerical simulation of the dynamic impact breakage testing of rock. *Int J Rock Mech Min Sci.* 2005;42(2):167-176.

Rehbock-Sander M, Jesel T. Fault induced rock bursts and micro-tremors–experiences from the Gotthard base tunnel. *Tunn Undergr Space Technol.* 2018;81:358-366.

Richter B, Stünitz H, Heilbronner R. The brittle-to-viscous transition in polycrystalline quartz: An experimental study. *J Struct Geol.* 2018;114:1-21.

Scott TE, Nielsen KC. The effects of porosity on the brittle-ductile transition in sandstones. *J Geophys Res Solid Earth*. 1991;96(B1):405-414.

Song B, Chen W. Loading and unloading split Hopkinson pressure bar pulse-shaping techniques for dynamic hysteretic loops. *Exp Mech.* 2004;44(6):622-627.

Wang M, Zhu ZM, Dong YQ, Zhou L. Study of mixed-mode I/II fractures using single cleavage semicircle compression specimens under impacting loads. *Eng Fract Mech.* 2017;177:33-44.

Wang QZ, Li W, Xie HP. Dynamic split tensile test of flattened Brazilian disc of rock with SHPB setup. *Mech Mater.* 2009;41(3):252-260.

Wasantha PL, Ranjith PG. Water-weakening behavior of Hawkesbury sandstone in brittle regime. *Eng Geol.* 2014;178:91-101.

Whittles DN, Kingman S, Lowndes I, Jackson K. Laboratory and numerical investigation into the characteristics of rock fragmentation. *Miner Eng.* 2006;19(14):1418-1429.

Wu BB, Yao W, Xia KW. An experimental study of dynamic tensile failure of rocks subjected to hydrostatic confinement. *Rock Mech Rock Eng.* 2016;49(10):3855-3864.

Xia KW, Yao W. Dynamic rock tests using split Hopkinson Kolsky bar system–A review. *J Rock Mech Geotech Eng.* 2015;7(1):27-59.

Xie HP, Sanderson DJ. Fractal effects of crack propagation on dynamic stress intensity factors and crack velocities. *Int J Fract.* 1996;74(1):29-42.

Xie HP, Zhu JB, Zhou T, Zhang K, Zhou CT. Conceptualization and preliminary study of engineering disturbed rock dynamics. *Geomech. Geophys Geo-energ Geo-resour.* 2020;6:34.

Xie HP, Zhu JB, Zhou T, Zhao J. Novel three-dimensional rock dynamic tests using the true triaxial electromagnetic Hopkinson bar system. *Rock Mech Rock Eng.* 2021;54:2079-2086.

Xu SL, Shan JF, Zhang L, Zhou LJ, Gao GF, Hu SS, Wang PF. Dynamic compression behaviors of concrete under true triaxial confinement: An experimental technique. *Mech Mater.* 2020;140:103220.

Yuan FP, Prakash V, Tullis T. Origin of pulverized rocks during earthquake fault rupture. *J Geophys Res Solid Earth*. 2011;116(B06309):1-18.

Zhang QB, Zhao J. Determination of mechanical properties and full-field strain measurements of rock material under dynamic loads. *Int J Rock Mech Min Sci.* 2013;60:423-439.

Zhang QB, Zhao J. A review of dynamic experimental techniques and mechanical behaviour of rock materials. *Rock Mech Rock Eng.* 2014;47(4):1411-1478.

Zhao H, Gary G. On the use of SHPB techniques to determine the dynamic behavior of materials in the range of small strains. *Int J Solids Struct.* 1996;33(23):3363-3375.

Zhao J, Cadoni E. Triaxially compressed Hopkinson bar (TriHB) for geomaterial and construction material testing. Proposal Submitted to the Swiss National Science Foundation (SNSF), 2009, No. 206021_128734, EPFL, Switzerloand.

Zhao J, et. al., Three dimensionally compressed and monitored Hopkinson bar. Australian Research Council, ARC LIEF (No. LE150100058), 2015, granted in 2016, Monash University, Australia.

Zhou YX, Xia KW, Li XB, Li HB, Ma GW, Zhao J, Zhou ZL, Dai F. Suggested methods for determining the dynamic strength parameters and mode-I fracture toughness of rock materials. *Int J Rock Mech Min Sci.* 2012;49:105-112.

Zhou T, Dong SL, Zhao GF, Zhang R, Wu SY, Zhu JB. An experimental study of fatigue behavior of granite under low-cycle repetitive compressive impacts. *Rock Mech Rock Eng.* 2018;51(10):3157-3166.

Zhou T, Zhu JB, Xie HP. Mechanical and volumetric fracturing behaviour of three-dimensional printing rock-like samples under dynamic loading. *Rock Mech Rock Eng.* 2020;53:2855-2864.

Zhu JB, Liao ZY, Tang CA. Numerical SHPB tests of rocks under combined static and dynamic loading conditions with application to dynamic behavior of rocks under in situ stresses. *Rock Mech Rock Eng*. 2016;49(10):3935-3946.

Zhu JB, Zhou T, Liao ZY, Sun L, Li XB, Chen R. Replication of internal defects and investigation of mechanical and fracture behaviour of rock using 3D printing and 3D numerical methods in combination with X-ray computerized tomography. *Int J Rock Mech Min Sci.* 2018a;106:198-212.

Fig. 1 Dynamic true triaxial electromagnetic Hopkinson bar (DTEHB) system: (a) Overall system configuration; (b) Three key components of the 3D centering and leveling system

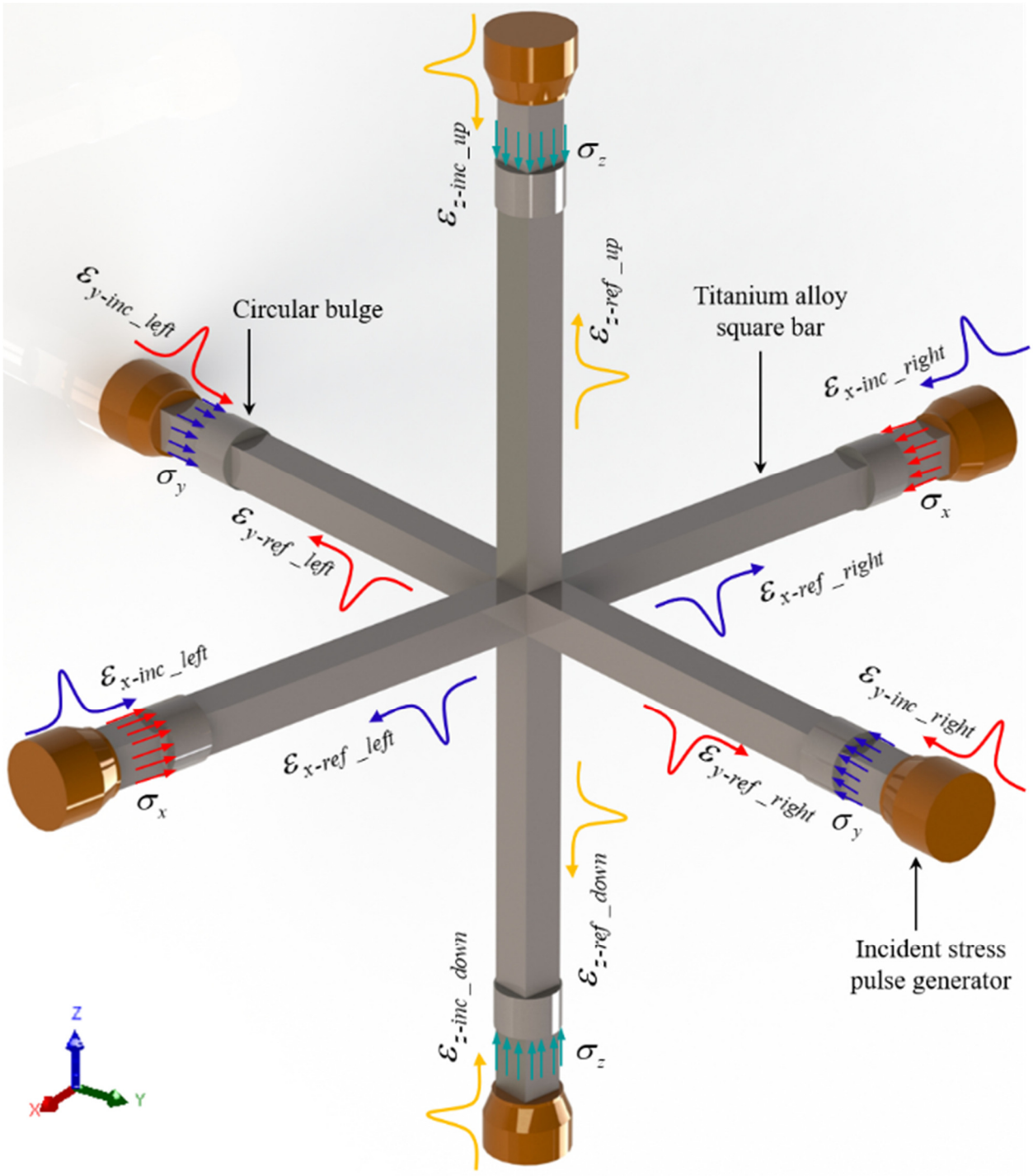

Fig. 2 Schematic diagram of stress state and wave propagation in the triaxial bars

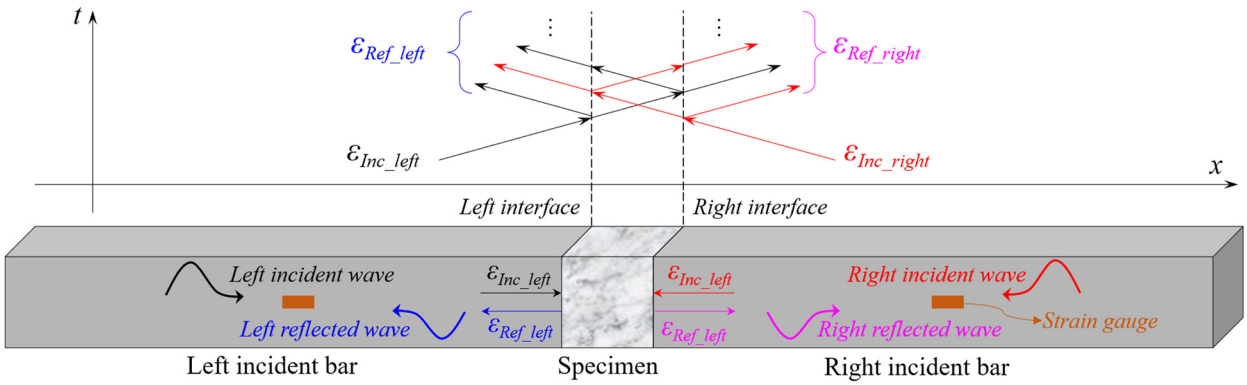

Fig. 3 Schematic diagram of wave propagation along the *x*-axis under conditions of symmetric loading

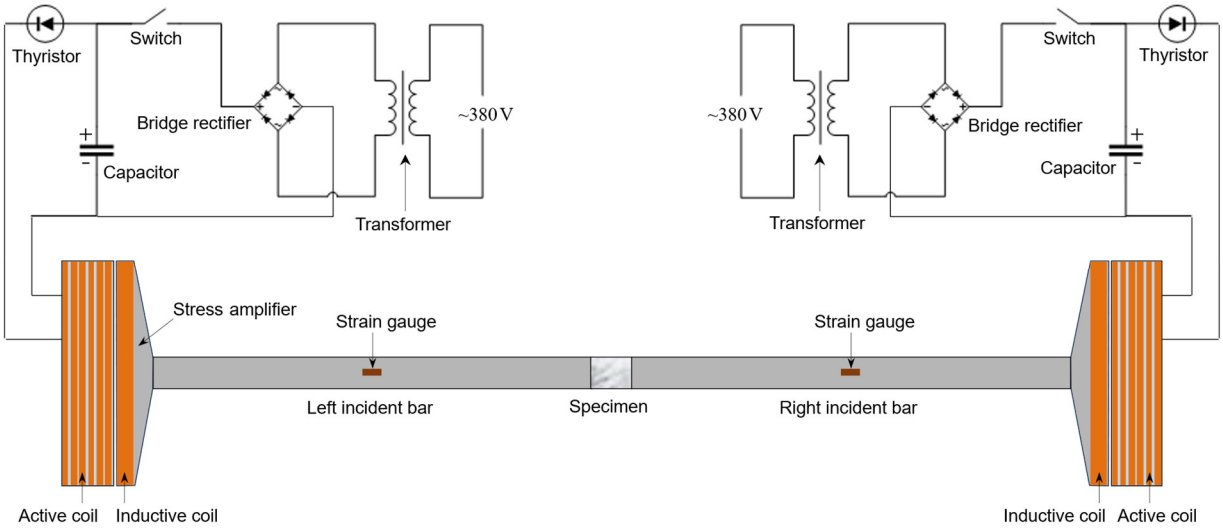

Fig. 4 Schematic diagram of electromagnetic stress pulse generation system in each axis

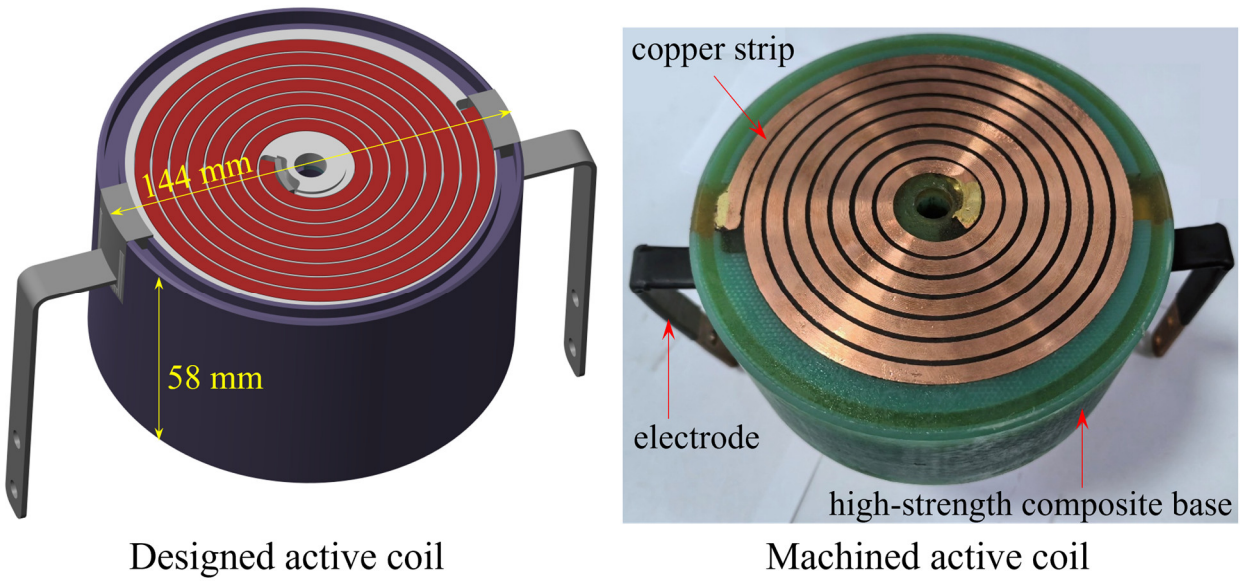

Fig. 5 3D structure of an active coil

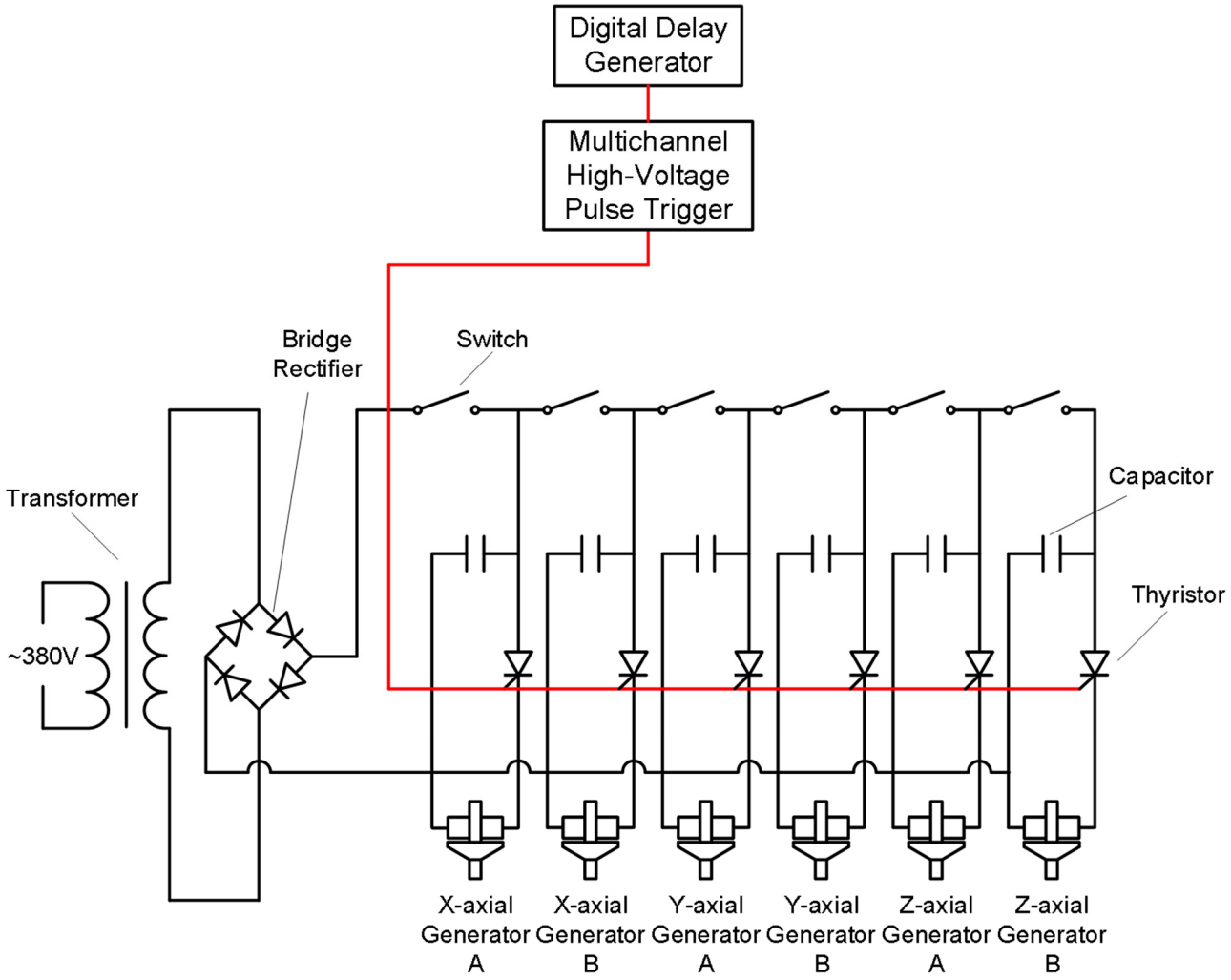

Fig. 6 Schematic diagram of the synchronous pulse control system

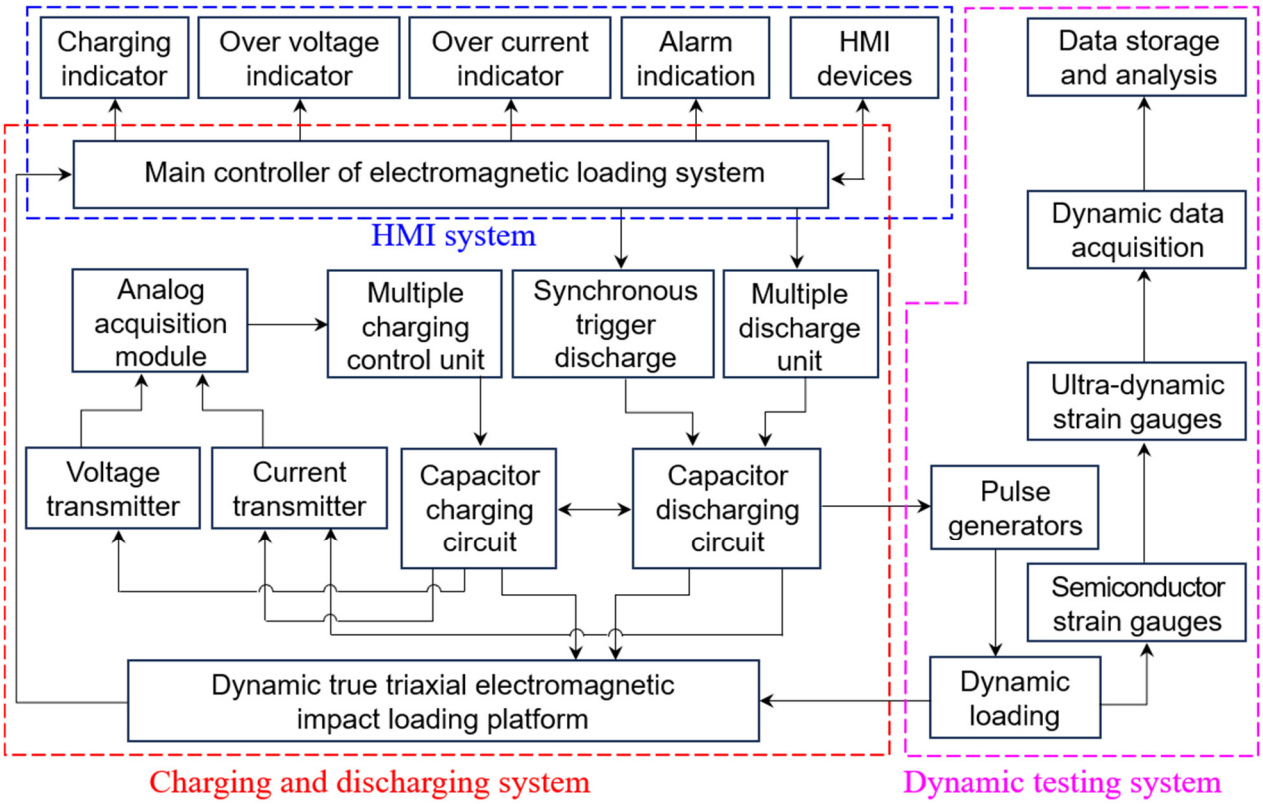

Fig. 7 Principle of the central control system

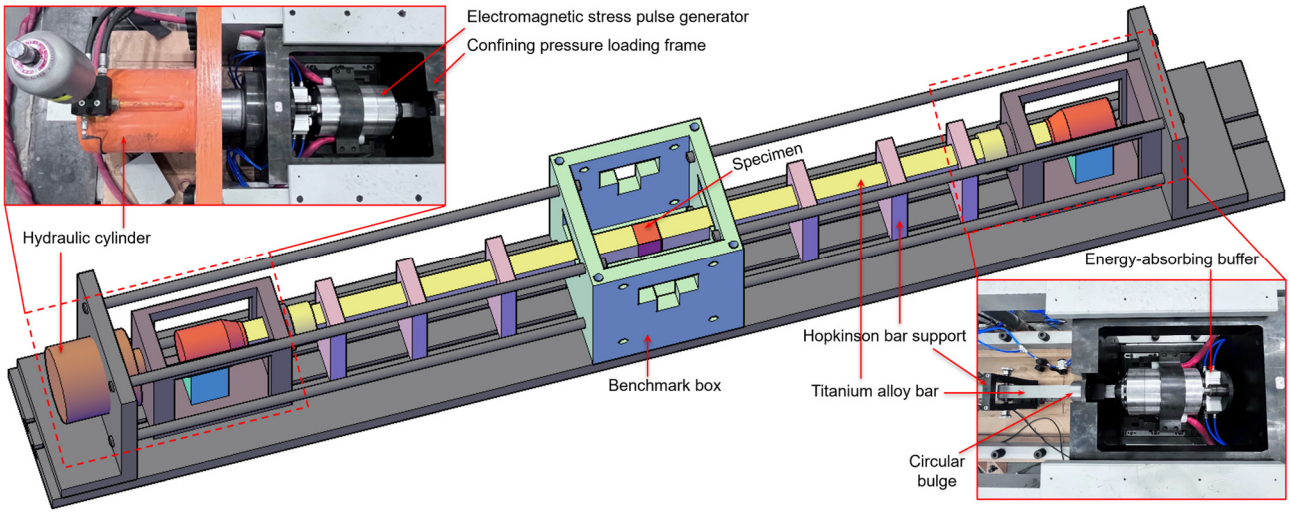

Fig. 8 Primary structural frame and static confining pressure loading system in one axis

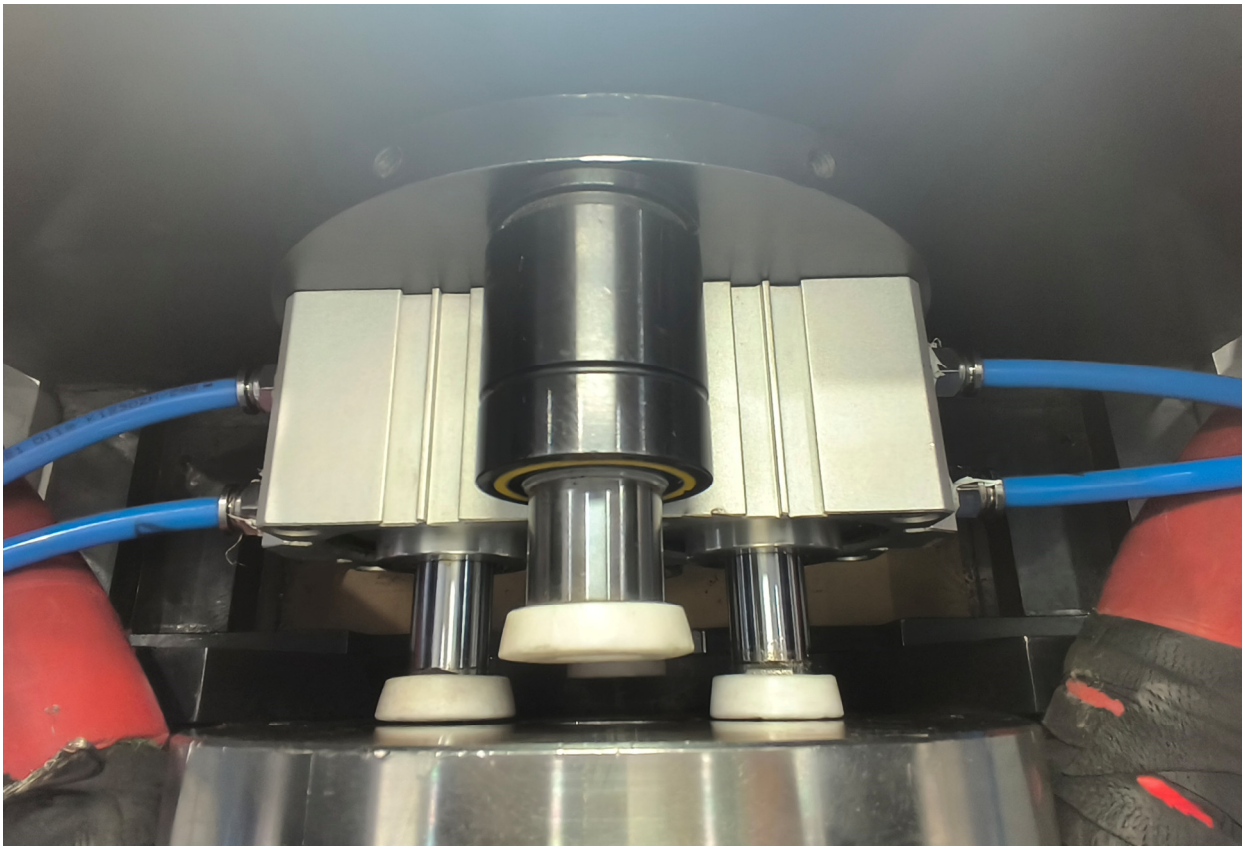

Fig. 9 Energy-absorbing buffer with self-resetting capability

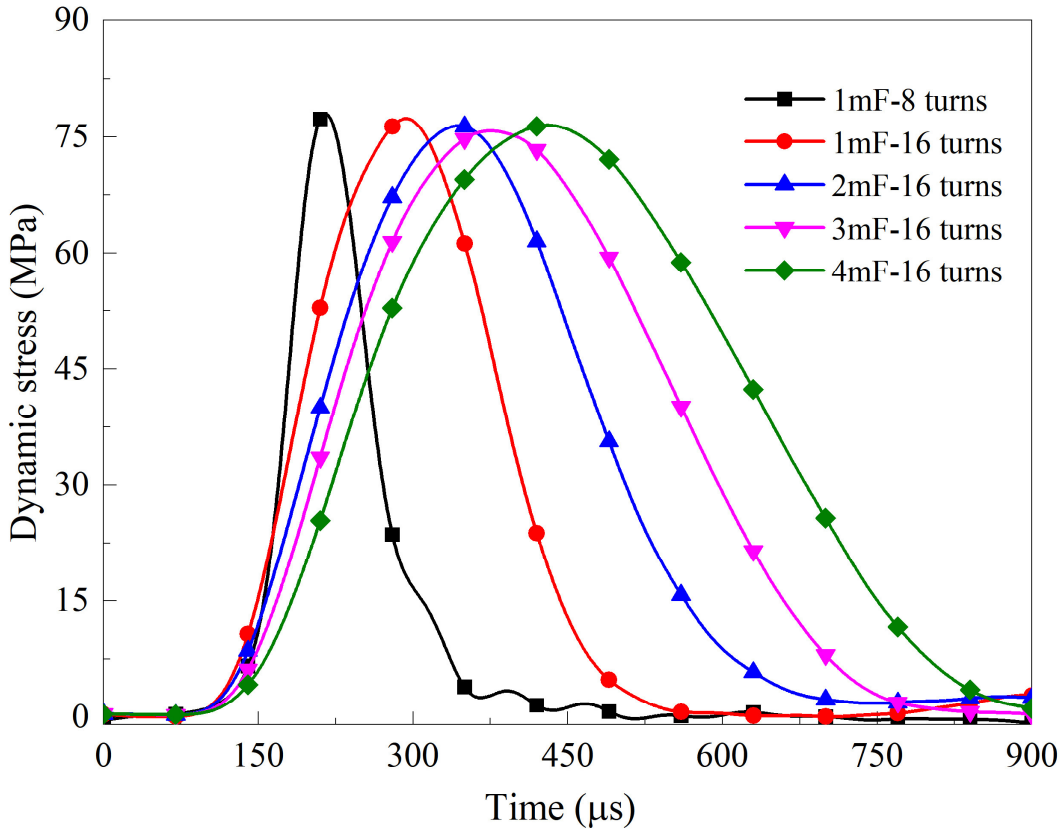

Fig. 10 Controllable and adjustable of stress wave durations generated by the ESPG

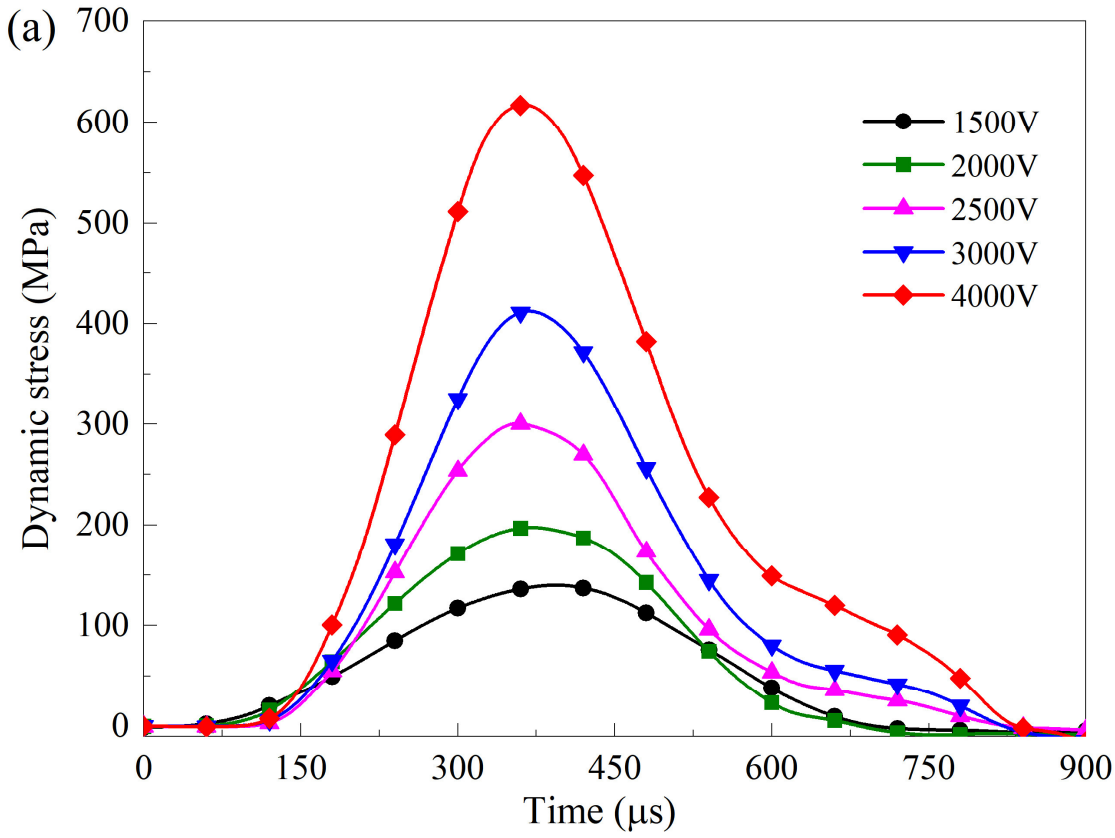

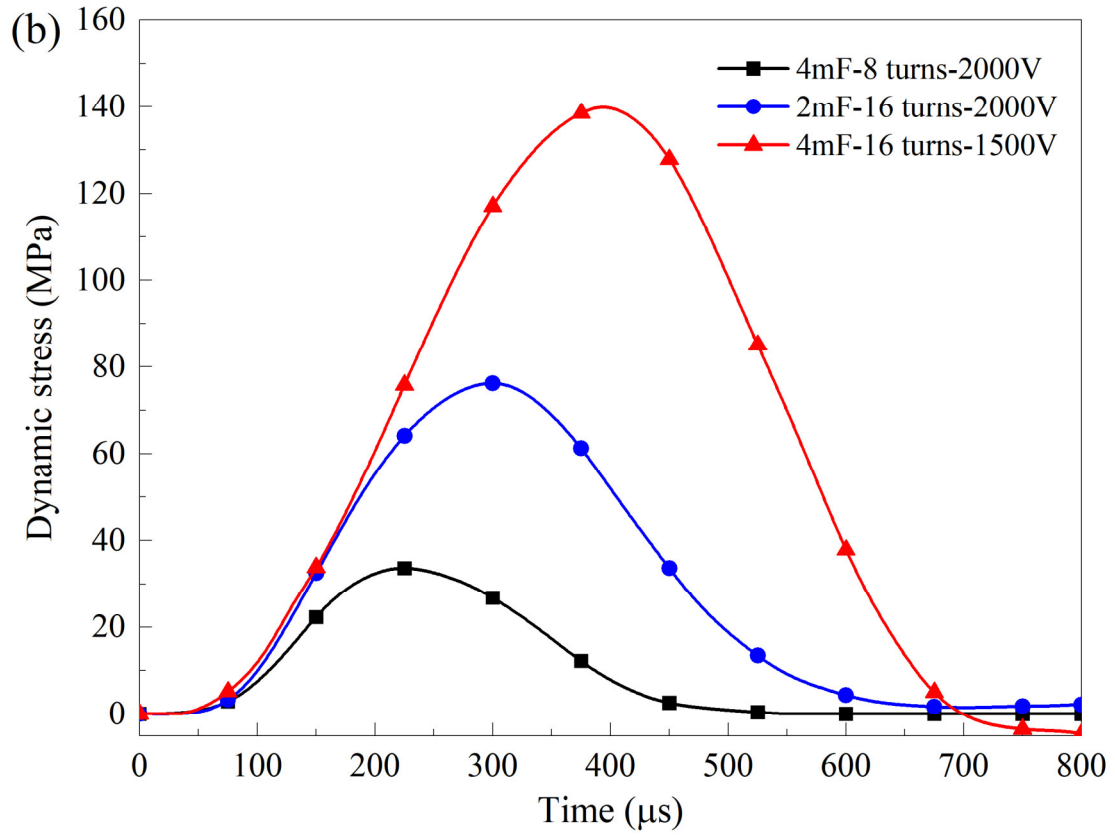

Fig. 11 Controllable and adjustable of stress wave amplitudes generated by the ESPG. (a) Effect of charging voltages on stress wave amplitude; (b) Influence of capacitance and active coil turns on stress wave amplitude.

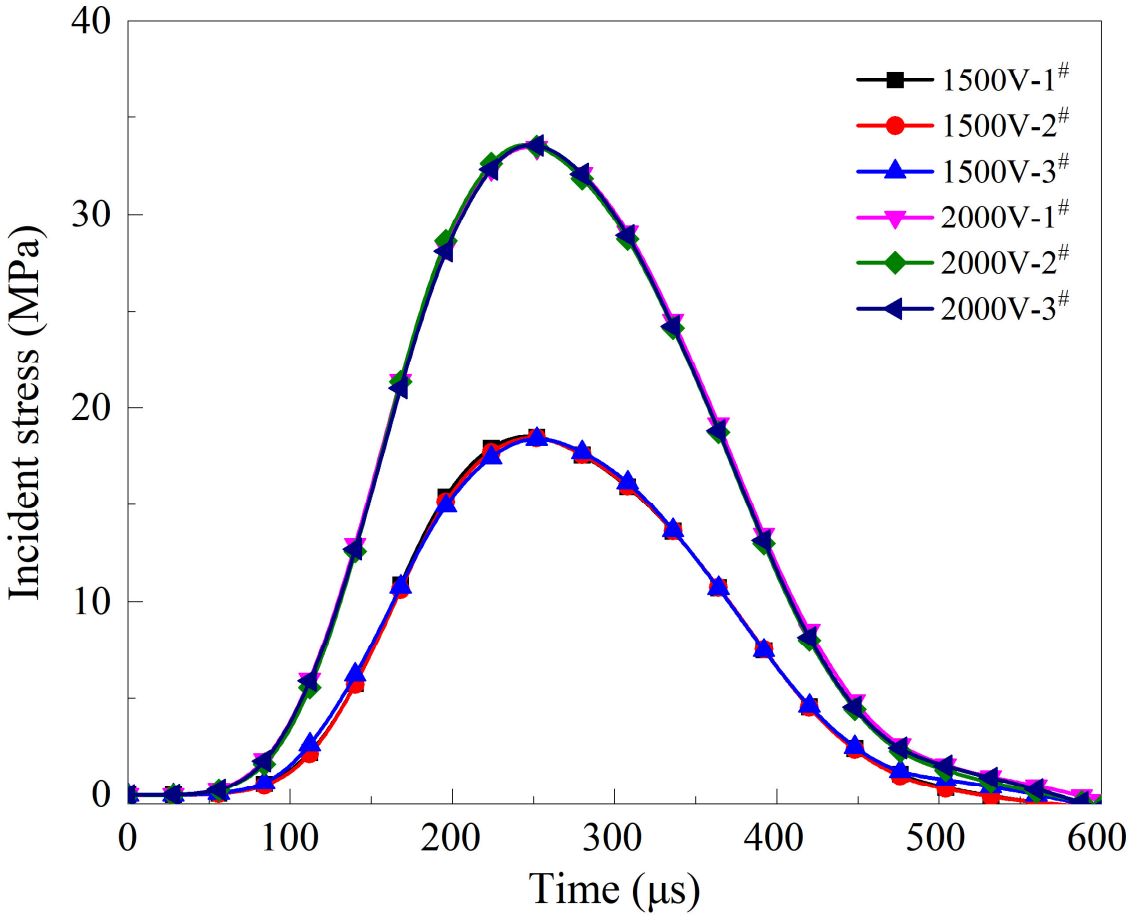

Fig. 12 Repeatability of stress waves generated by the ESPG

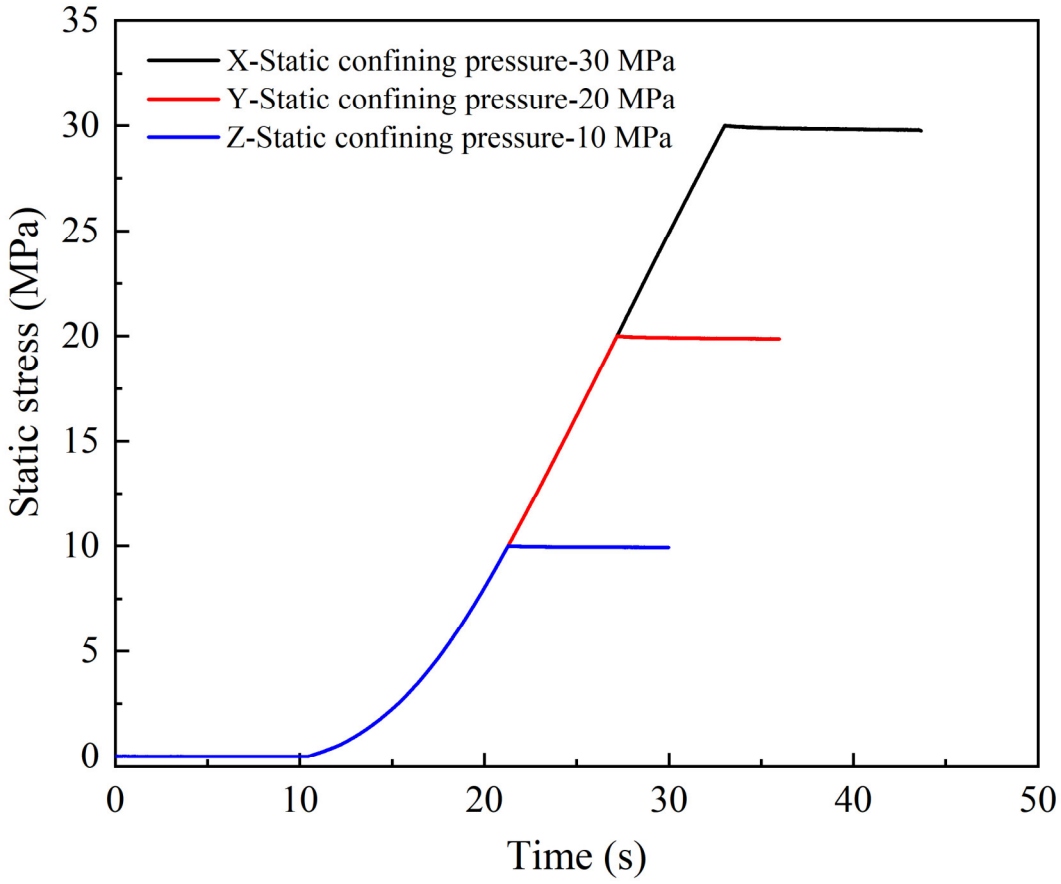

Fig. 13 Application of static confining pressures along each axis

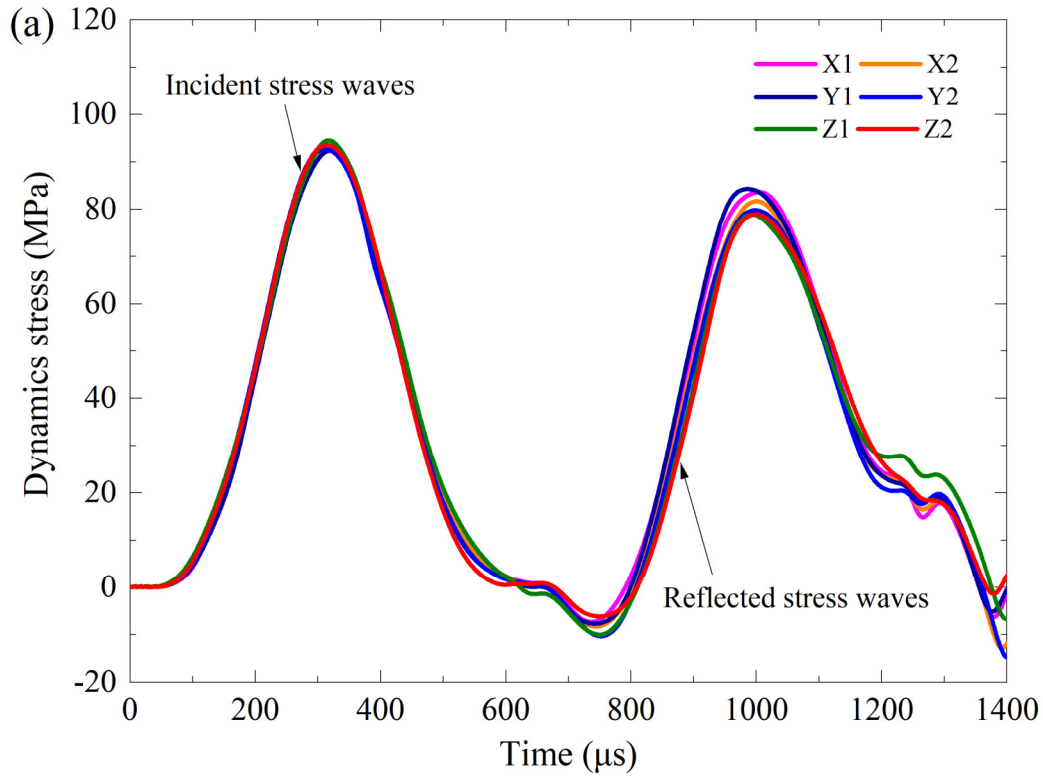
(a)
Incident stress waves
Reflected stress waves
X1
X2
Y1
Y2
Z1
Z2
Dynamics stress (MPa)
Time (μs)
120
100
80
60
40
20
0
-20
0
200
400
600
800
1000
1200
1400

1

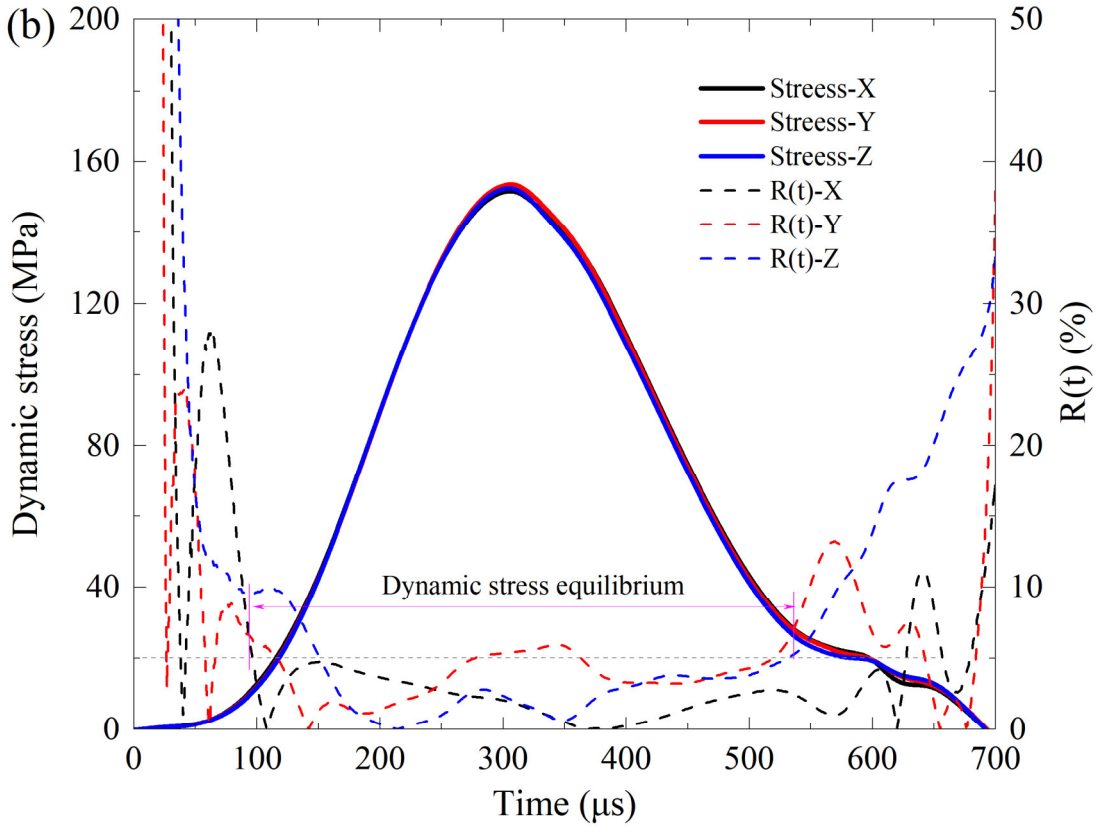
(b)
Streess-X
Streess-Y
Streess-Z
R(t)-X
R(t)-Y
R(t)-Z
Dynamic stress equilibrium
Dynamic stress (MPa)
R(t) (%)
Time (μs)
200
160
120
80
40
0
50
40
30
20
10
0
0
100
200
300
400
500
600
700

2

3

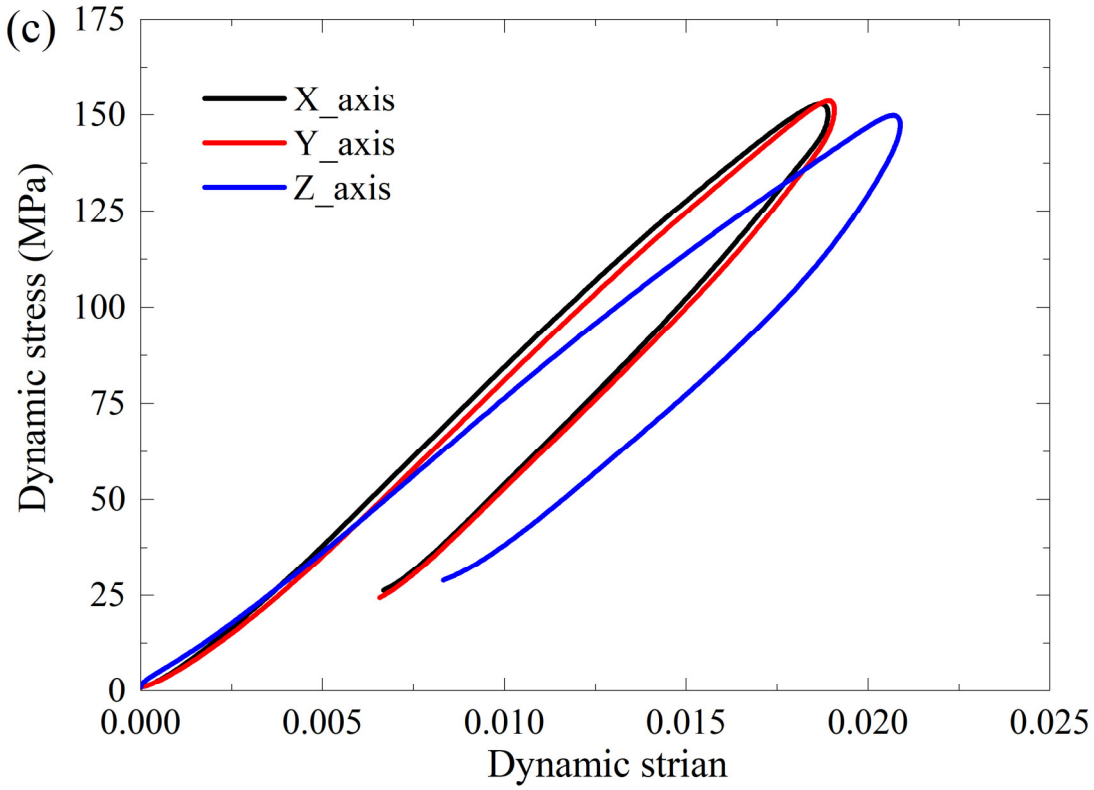

Fig. 14 A typical dynamic true triaxial impact test of a coal specimen. (a) Incident strain signals measured on the triaxial bars; (b) Dynamic stress balance in each axis; (c) Dynamic stress-strain curves in the X, Y and Z axes of the coal specimen.

Table 1 Summary of the techniques, equipment and objectives for data acquisition and analysis

Signals	Technique	Equipment	Objectives
Dynamic strain	Synchronous signal acquisition technology	Multi-channel dynamic strain recorder	To derive dynamic stress-strain curves; analyzing dynamic mechanical properties, e.g., dynamic strength and strain
Surface fracturing	High-speed photogrammetry	Ultra-high-speed camera	To obtain crack propagation velocity; analyzing crack nucleation, initiation, propagation, coalescence and failure modes
3D fracturing, deformation	High-speed photogrammetry, 3D DIC technique	High-speed cameras, DIC analysis software	To analyze 3D fracturing type, behavior and mechanism; analyzing full field deformation and its localization and evolution
Surface temperature evolution	High-speed infrared thermography	High-speed infrared thermal camera	To characterize rock fracture thermomechanics; analyzing real-time temperature evolution, fracture-zone thermal fields, and energy dissipation
Acoustic emission (AE)	AE detection technology	AE probe, AE detector	To analyze dynamic damage and fracturing mode of the specimen
Macro- and meso-cracks	X-ray computed tomography (CT)	High-resolution X-ray CT	2D and 3D damage and fracture network inside opaque materials; spatial evolution of micro- and macro-crack inside the specimen
Meso- and micro-cracks	Scanning electron microscope	Scanning electron microscope	Microcrack characteristics; failure mechanism of the specimen at microscopic scale